# QUANTUM EFFECTS
# IN MgO-BASED
# MAGNETIC TUNNEL JUNCTIONS

DO BANG

SEPTEMBER 2010

# QUANTUM EFFECTS
# IN MgO-BASED
# MAGNETIC TUNNEL JUNCTIONS

A dissertation submitted to

**THE GRADUATE SCHOOL OF ENGINEERING SCIENCE,**

**OSAKA UNIVERSITY**

In partial fulfillment of the requirements for the degree of

DOCTOR OF PHILOSOPHY IN ENGINEERING

BY

DO BANG

SEPTEMBER 2010

# ABSTRACT

The tunnel magnetoresistance (TMR) effect in a magnetic tunnel junction (MTJ) with a crystalline MgO(001) tunnel barrier (MgO-based MTJ) is especially important because of the large magnetoresistance at room temperature and the applications for new generation spintronics devices. The TMR effect is also known to be sensitive to layer interfaces due to quantum effects such as a scatter or interference of tunneling electrons. This dissertation contributes towards the investigation of quantum effects in the MgO-based MTJs as described bellow.

Chapter 1 provides a detailed introduction of MgO-based MTJs and its quantum effects, followed by purposes of this study. Chapter 2 then describes the fabrication of the MTJs and experimental methods used in this dissertation. The experimental results and discussion are shown in Chapter 3 which consists of four sections: (1) In Sec. 3.1, the properties of Kondo effect was investigated for both single crystal MTJs and the MTJs with the boron-doped top ferromagnetic electrode in order to find out the origin of the Kondo effect. The experimental results suggested that magnetic impurities (Fe, Co or Mn) diffused into the MgO barrier through defects could be an origin of the effect. (2) In Sec. 3.2, deals with investigations of bias and temperature dependences of conductance arising from the magnon contribution in MgO-based MTJs. A series of experimental results proposes an important role of the surface (2D) magnon excitation. (3) In Sec. 3.3, the process of preparation of epitaxial MTJs with ultrathin Fe electrodes is reported. These samples show a strong quantum resonant effect as a clear oscillation of dynamics conductance with the bias-voltage and energy of quantum well states strongly depends on the ultrathin-Fe thickness. (4) The results also opened a new research topic of contribution of quantum well states to spin-torque diode spectrum in epitaxial MgO-based MTJs as reported in Sec. 3.4.

Finally, conclusions of origins of Kondo, magnon and also quantum interference effects and their contributions to tunneling transport properties of the MgO-based MTJs are discussed in Chapter 4. Especially, it is suggested that the TMR and spin-torque can be significantly influenced and modulated by the QW states.

# CONTENTS

# Chapter 1. INTRODUCTION

## 1. 1. MgO-based magnetic tunnel junctions

It is well known that quantum tunneling effect refers to the phenomenon of an ability of a particle to penetrate an energy barrier within electric structure. Some devices that exploit this property are known as tunneling junctions and are made by sandwiching an extremely thin (~ few nm) insulating layer between two conducting layers. In 1975, Michael Julliere discovered that if ferromagnetic materials were used as the conducting layers in such a junction, so-called magnetic tunnel junction (MTJ), then its conductance would depend on magnetic configurations of two ferromagnetic (FM) electrodes or the magnitude of the applied field (Figure 1.1)[1]. The conductance of the MTJ for parallel configuration, $G_P$, is larger than that for antiparallel configuration, $G_{AP}$. This change in conductance with the relative magnetization direction of two FM layers, called the tunneling magnetoresistance effect, revived large interest in the MTJs due to the overwhelming success of other magnetoresistive technologies for magnetic sensing applications. The magnitude of the effect is estimated by the tunneling magnetoresistance (TMR) ratio, which is defined as $(G_P-G_{AP})/G_{AP}$, (Figure 1.2). Using experimentally estimated spin polarizations of various FM materials, TMR ratios as high as about 70% are predicted for MTJs using Al-O barriers. These values have been confirmed experimentally by many groups around the world.[2-4]

In 2001, two groups separately predicted that TMR values as high as 1000% could be attained if properly-grown, crystalline MgO(001) and two Fe(001) layers were used as the insulating barrier and ferromagnetic electrodes, respectively.[5,6] The explanation for such a large TMR ratio relies on the coherence of electrons tunneling through the barrier. With an amorphous insulator, the momentum of a tunneling electron is not conserved, due to scattering within the barrier or interfaces, and any coherence or symmetry of conducting electrons is destroyed. However, in the MgO(001) insulator layer whose symmetry is $C_{4V}$, which is the same as that of the ferromagnetic electrodes, with the symmetry axis normal to the layer. In addition, MgO(001) and Fe(001) lattices make a lattice matched coherent interface. Therefore, in-plane momentum, $\vec{k}_{//}$ and orbital symmetry are conserved during the tunneling process. Since MgO has its band gap minimum at Γ-point, evanescent states as $\overline{\Gamma}$-point shows minimum decay rates in the local density of states, which further strongly depends on the orbital symmetries ($\Delta_1$, $\Delta_2$, $\Delta_2'$, $\Delta_5$). In MgO at $\overline{\Gamma}$ the lowest decay rate is expected for $\Delta_1\left(s-p_z-d_{3z^2-r^2}\right)$ hybridized states. In Fe layer,

the band blanch with $\Delta_1$ symmetry is 100 % spin-polarized (Figure 1.3b). As a result, the difference in conductance between the parallel and antiparallel configurations is greatly enhanced (Figure 1.4).

Large TMR values using MgO-based MTJs were confirmed by two groups in 2004 when TMR values of ~200% at room temperature were reported.[7,8] Over time, TMR values at room temperature reach as high as 500 %.[9-11] Because of the enormous TMR ratios, the MgO-based MTJs are widely used in read heads for hard disc drive and magnetic random access memory (MRAM), and they will become the dominant magnetic sensing technology in years to come. The achievement of the TMR, however, is characterized by a discrepancy of one or two orders of magnitude between obtained experimentally low and theoretically high values of the TMR ratio.[12,13] The origin of that discrepancy is related to the junction quality, especially the crystallinity and homogeneity of the barrier, and to the crucial role of the interface structure for the tunneling probability.[14] A high density of structure defects, rough interfaces, and amorphous barriers cause strong scattering even in ballistic regime. The Kondo effect and an inelastic scattering of electrons due to magnon excitation and adsorption are also reducing in TMR of MTJs.[15-17] In Sec. 1.2 and Sec. 1.3, the backgrounds of these effects are shown in detail.

The coherent tunneling in the crystalline MgO-based MTJs may contribute to not only large achieved TMR but also to another quantum phenomenon: spin-polarized resonant tunneling. The effect is simply realized by inserting an ultrathin non-magnetic (NM)/ferromagnetic (FM) metal layer between the insulating barrier and one of the two electrodes of a MTJ.[18-20] The quantum resonant state is expected to enhance the TMR at the bias voltage corresponding to its energy as well as a spin-transfer torque, which can induce various phenomena such as magnetization switching, spin-torque diode effect, and spin-torque-induced oscillation.[21-24] Reviews of the research on these effects are described in Sec. 1.4 and Sec. 1.5. Besides investigations of the quantum resonance effect and its contribution to properties of MTJs, studies on Kondo and magnon effects are also purposes of the dissertation and introduced in Sec. 1.6.

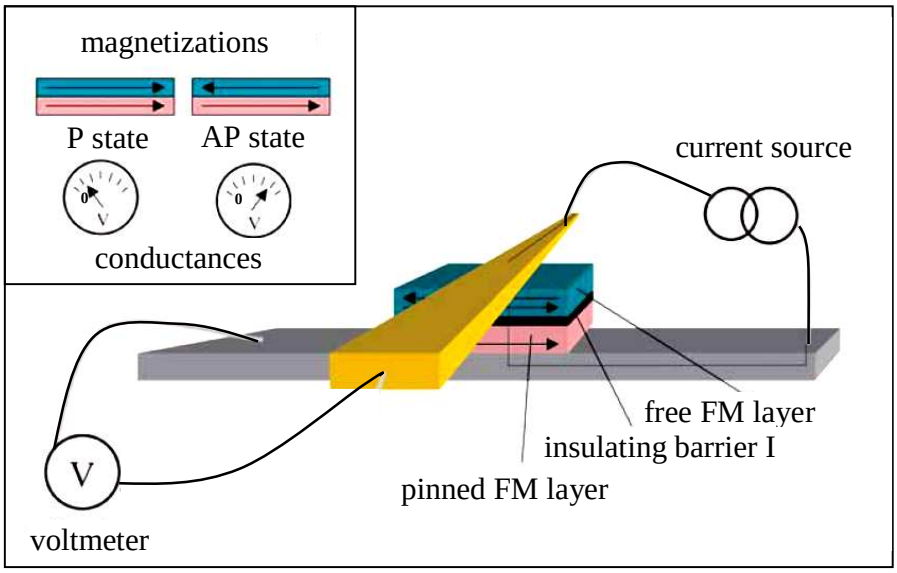


***Fig. 1.1***

*Schematic of a magnetic tunneling junction (MTJ): The magnetization of the pinned layer is fixed and the magnetization of the free layer can be switched by applying an external magnetic field. Inset: (a) Magnetizations in the two FM layers are aligned parallel (P state) and (b) antiparallel (AP state) which correspond to two states of junction resistance as well as conductance.*

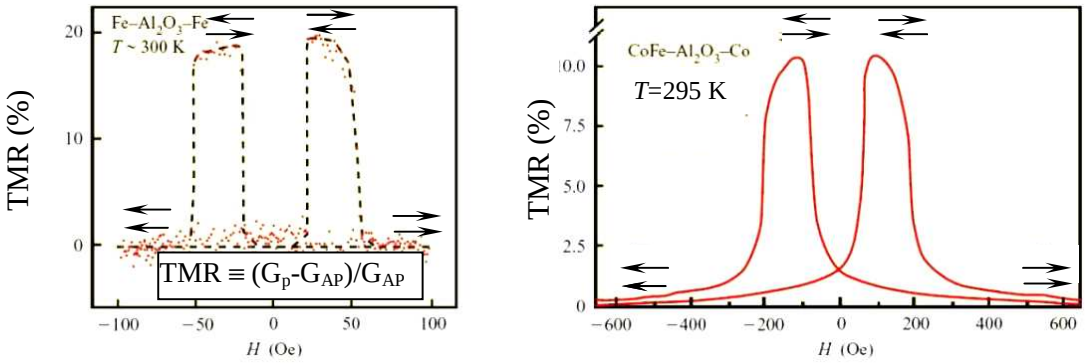


***Fig. 1.2***

*Collection of early experimental evidences about TMR: Miyazaki and Tezuka (left) and Moodera (right), adapted from Ref. [2] and [3] respectively.*

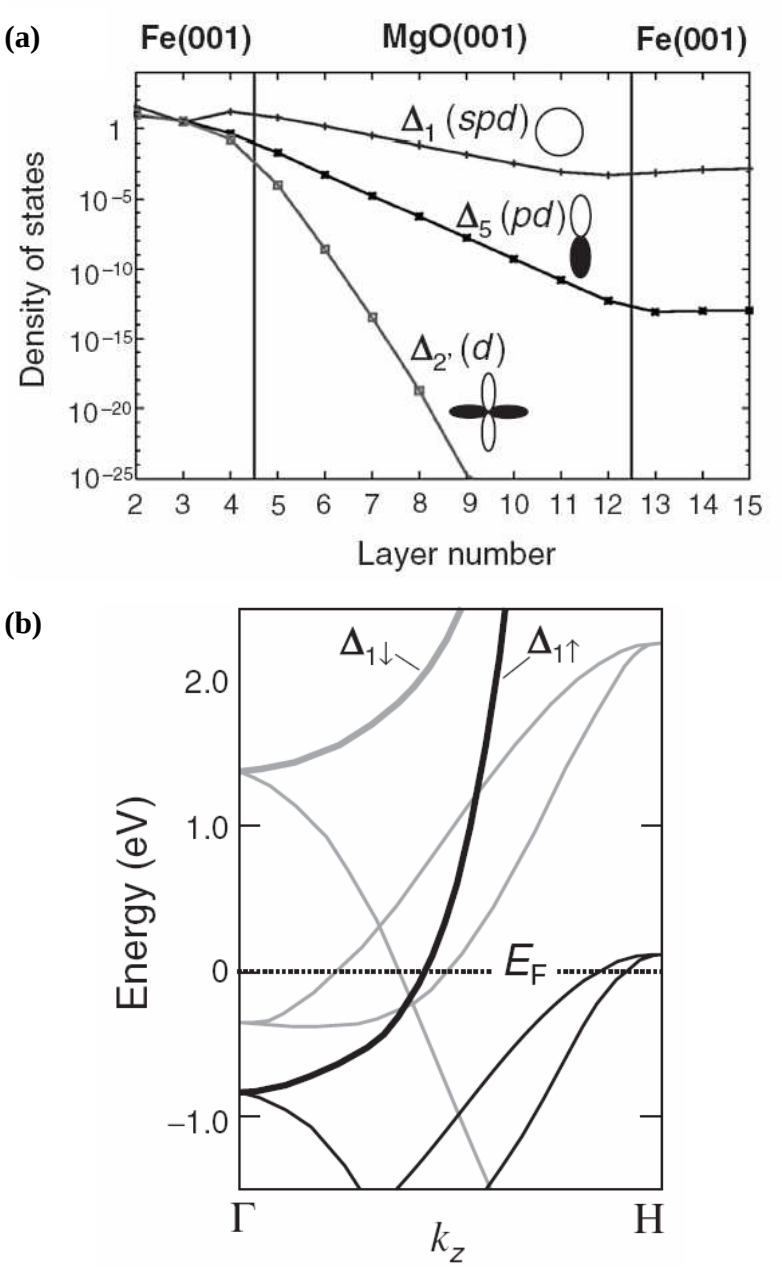


***Fig. 1.3***

*(a) Coupling of wave functions between the Bloch states in Fe and the evanescent states in MgO and tunneling density of states of majority-spin states for $k_{//} = 0$ in Fe(001)/MgO(001)/Fe(001) with parallel magnetic state. (b) Band dispersion of bcc Fe in the [001] (Γ–H) direction. Black and gray lines respectively represent majority- and minority-spin bands. Thick black and gray lines respectively represent majority- and minority- spin $\Delta_1$ bands. $E_F$ denotes Fermi energy, adapted from Ref. [5].*

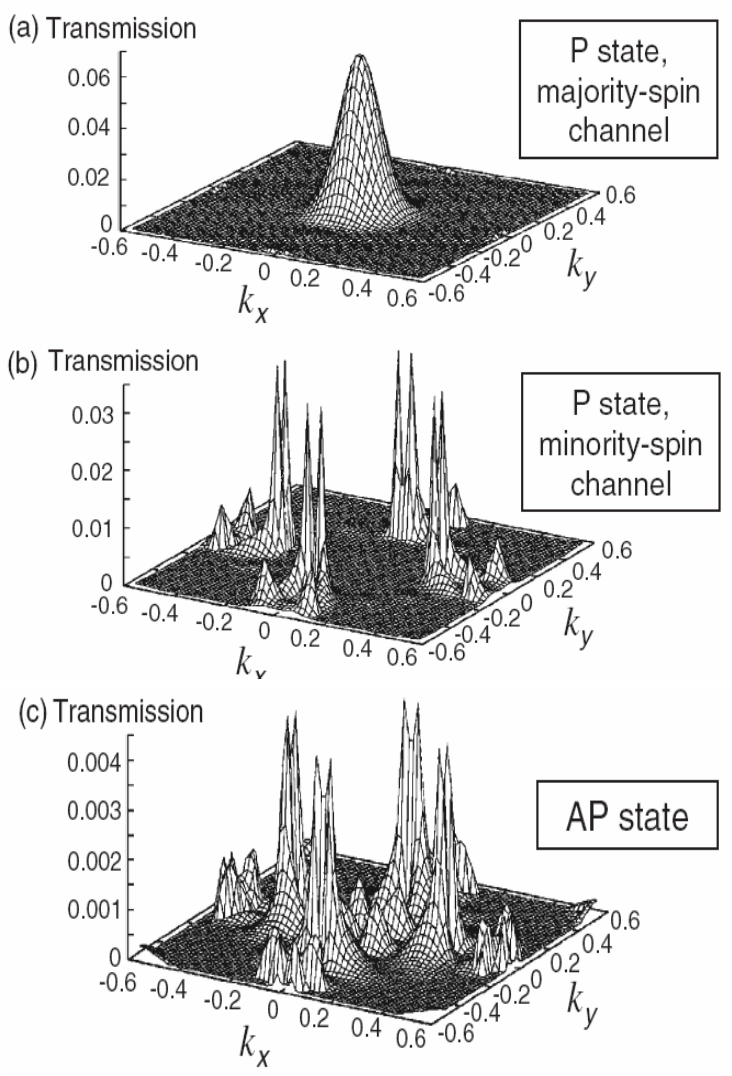


***Fig. 1.4***

*Tunneling probability in a Fe(001)/MgO(001)(4 ML)/Fe(001) MTJ as a function of $k_x$ and $k_y$ wave vectors (ML: mono-atomic layer). (a) Majority-spin conductance channel in the parallel magnetic state (P state), (b) minority spin conductance channel in the P state, and (c) conductance channel in the antiparallel magnetic state (AP state), adapted from Ref. [5].*

### 1.2. Contributions of Kondo effect to transport properties of MTJs

A single magnetic atom, which is diluted into a nonmagnetic host, is often referred as a Kondo impurity. The localized spin of a Kondo impurity interacts with the spin of surrounding conduction electrons, resulting in anomalous transport properties in the dilute magnetic alloy. This phenomenon, known as the Kondo effect, causes the strong temperature dependence of measurable resistance at low temperatures (Figure. 1.5).[15] In the milestone work of Kondo, for a single impurity the calculation of the electrical resistivity was estimated by introducing a Kondo Hamintonian of the form,[16]

$$H_{\text{int}} = J\,\vec{S}_I \cdot \vec{s}_c(0) \qquad \text{(Eq. 1.1)}$$

where $\vec{S}_I$ is the impurity spin, $\vec{s}_c(0)$ is the conduction electron spin density at the impurity site and J magnetic exchange coupling. Note that positive J corresponds to antiferromagnetic coupling, and negative J to ferromagnetic coupling. Kondo's result was extended to third order in the local moment-conduction-electron exchange coupling J that the resistivity took the form[16]

$$\rho(T) = \rho_0(T) + aN(0)J^2 + bN(0)^2 J^3 \ln\left(\frac{D}{kT}\right), \qquad \text{(Eq. 1.2)}$$

where $\rho_0(T)$ is the resistivity of the pure metal, N(0) is the conduction-electron density of states at the Fermi energy, *D* is the bandwidth of the conduction-electron system (of the order of the Fermi energy), and *a* and *b* are constants and proportional to the impurity concentration.

In the last decades, Kondo effect has been extensively studied in both theoretical and experimental aspects.[25-29] Most these studies of the Kondo effect, however, have focused only on the case of a nonmagnetic host but not a magnetic metallic case. In nonmagnetic tunnel junctions the Kondo effect manifests itself as a zero-bias anomaly (ZBA) peak in the dynamic conductance or dynamic resistance depending on the position of the magnetic impurity in the nonmagnetic tunnel junctions. A great boost in understanding this effect came from studies on the X-ray absorption worked out theoretically by Mahan and more elaborately by Nozieres.[30] There are also a few studies of the influence of Kondo effect on the transport properties of magnetic tunnel junctions (MTJs),[31] which recently have much potential application to next generation spintronic devices such as ultrahigh density hard disk drives or magnetoresistive random access memory. In Ref. [31], authors have succeeded in studying the transport properties and providing experimental evidence for the observation of Kondo effect in Al-O based MTJs. It showed strongly suppressed TMR at low temperatures, more pronounced as thickness of Al-O

barrier is increased (Figure 1.6a), and strongly temperature dependent peak in dynamic junction resistance (Figure 1.6b). These are attributed to Kondo scattering of tunneling electrons by the magnetic impurities at the electrode-barrier interface. At temperatures below the Kondo temperature ($T_K$), the junction resistance is dominated by the Kondo scattering contribution such that the TMR is strongly suppressed.

Tunneling spectroscopy is known as a powerful tool for investigating the details of the tunneling process.[32,33] By measuring first and second derivative conductance ($dI/dV$, $d^2I/dV^2$) with an energy resolution down to sub meV, the effects of the density of states and inelastic scattering processes on conductance can be detected in detail.

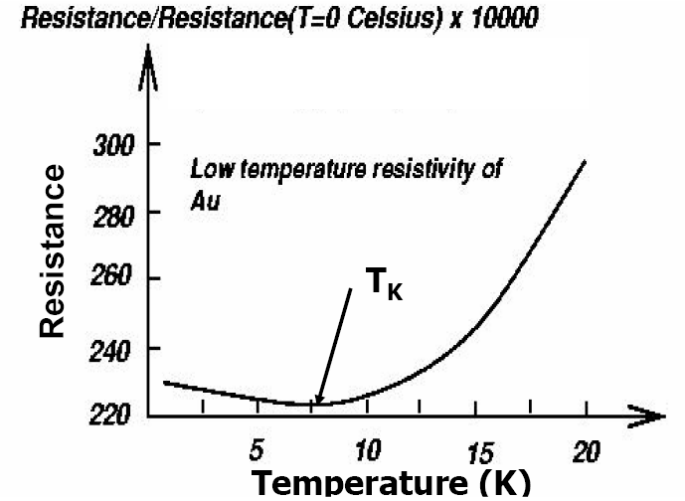


***Fig. 1.5***

*The temperature dependence of Au resistance including the Kondo effect shows a minimum at certain low temperature, Kondo temperature – $T_K$, adapted from Ref. [15].*

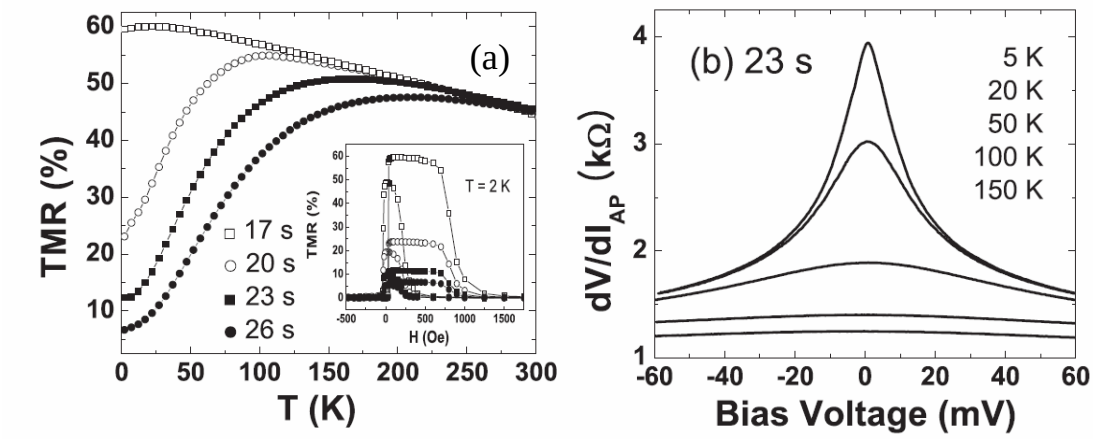


***Fig. 1.6***

*(a) Temperature dependences of TMR with different Al-O oxidation times (t = 17, 20, 23, 26 s) show a significant reduction of TMR at temperatures lower than $T_K$. The inset shows the TMR loops at 2 K for different Al-O oxidation times. (b) Dynamic resistance (antiparallel state) with varying temperatures for the MTJ with t = 23 sec shows zero bias anomaly (ZBA) peaks (adapted from Ref. [29]).*

### 1.3. Contributions of Magnon effect to transport properties of MTJs

The magnitude of the tunneling magnetoresistance ratio (TMR) at low temperatures nearly agrees with Julliere's simple model predictions. This model is based on the conservation on spins during tunneling process, the difference in the density of states (DOS) for the two spin directions at $E_F$ of the itinerant electrons in the FMs, and earlier results of spin polarized tunneling between a FM and a superconductor.[1] However, the TMR exhibits both a strong temperature ($T$) and *d.c.* bias ($V_{d.c.}$) dependences (Fig 1.7).[32,35] These effects are surprisingly significant and depend on the quality of the junctions; the lower the TMR, the larger the temperature and the *d.c.* bias dependence. Earlier, other reports have reported a few percent TMR at liquid helium temperatures, whereas at room temperature it was only (0–2) %. Likewise, junctions showed a factor of one order reduction in TMR when $V_{d.c.}$ was increased from 0 to 0.5 V.

Moodera *et al*. later found that inelastic scattering processes in the ferromagnetic electrodes of a magnetic tunnel junction are responsible for a reduction of the tunneling magnetoresistance effect at finite bias.[32] Then, the inelastic tunneling process of electrons in magnetic tunnel junctions (MTJs) was a subject of considerable interest. Because this process can cause spin flipping of the electrons as well as the generation and annihilation of magnons. Therefore, that tunneling process may violate spin conservation and lead to a decrease of the optimal tunneling magnetoresistance.[34] In the report Ref. [36], T. Bratkovsky *et al.* discussed which hot electrons can inelastically create magnons using quantum-mechanical selection rules for magnon creation. It was assumed that the spin-orbit interaction in the ferromagnet is weak such that the total spin is a conserved quality. So the magnon creation mechanism can be described as follows.

When a positive sample bias U is applied to the ferromagnetic electrode, electrons tunnel into the ferromagnetic resulting in hot electrons above the Fermi level $E_F$. The hot electrons thermalize in the electrode by scattering with lattice defects, phonons, or other electrons. To flip the spin, a potential μ is required that couples the spin of the hot electrons to the spins of the ferromagnetic. As the hot electron is relatively close to $E_F$, the potential with the Ruderman-Kittel-Kasuya-Yosida (RKKY)-like exchange interaction can be approximated. To first order the traveling hot electron will scatter with the spin of the magnetization via this potential. The scattering cross section $\sigma$ of the hot electron can be calculated with the Born approximation from the interaction potential $\mu$ as the form[36]

$$\sigma(E) = |\mu[q(E)]|^2 D(E), \qquad \text{(Eq. 1.3)}$$

where, *q(E)* is the momentum transfer, i.e., the magnon momentum, and *D(E)* is the magnon density of states. The energy distribution of excited magnons can be obtained directly from the inelastic tunneling spectra (IETS).[32,33] In inelastic tunneling spectroscopy, a physical system is placed in the gap between two tunneling electrodes. When the tunneling electrons have enough kinetic energy $U = eV$ to excite an inelastic process in the physical system, the tunneling current $I$ is enhanced due to an increase of the number of final states. The onset of scattering creates a step in the differential conductivity $dI/dV$ or a peak in $d^2I/dV^2$. Inelastic excitation or only virtual excitation may occur, leading to peaks with odd or even symmetry in $V$ bias.

Many attempts have been made to find the contribution to the conductivity due to the magnons, excited by tunneling electrons in MgO-based MTJs by measuring the IETS.[37-39] It is so far believed that those spectra are originated by interface defects, and therefore, strongly depend on the sample quality. Therefore the barrier and the interfaces both are essential for the fabrication of tunnel junctions with high TMR values. In general the current transport in magnetic tunnel junctions is a complex superposition of different contributions. The study, understanding and control of these effects are the key to all future spintronics applications.

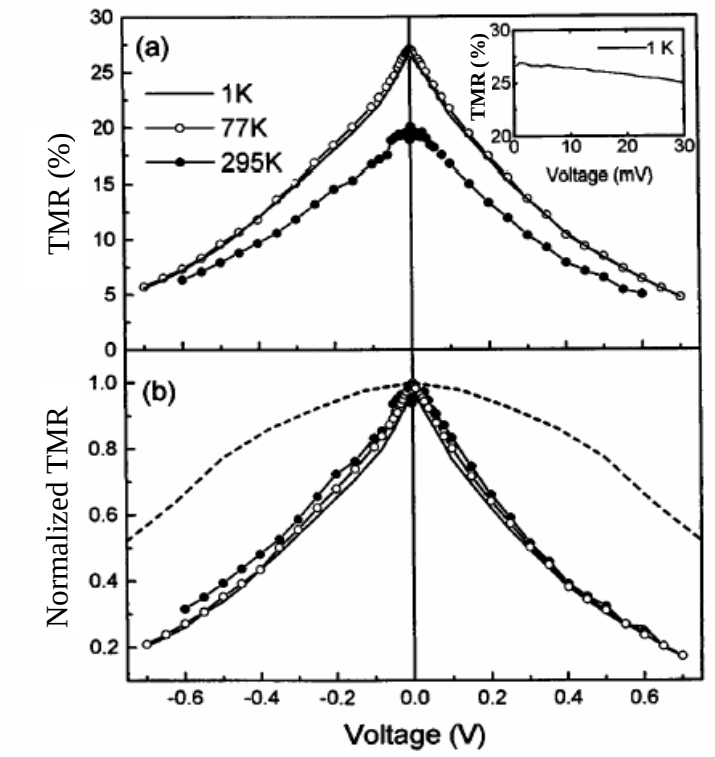


***Fig. 1.7***

*Bias dependences of TMR at three temperatures for Co/Al-O/NiFe junction: (a) The actual percentages and (b) normalized at zero bias. The inset shows the TMR in the low bias region displaying near constancy of TMR. The dashed line in (b) is the theoretically expected variation for a Fe/Al-O/Fe junction (from Fig. 1 in Ref. [35]).*

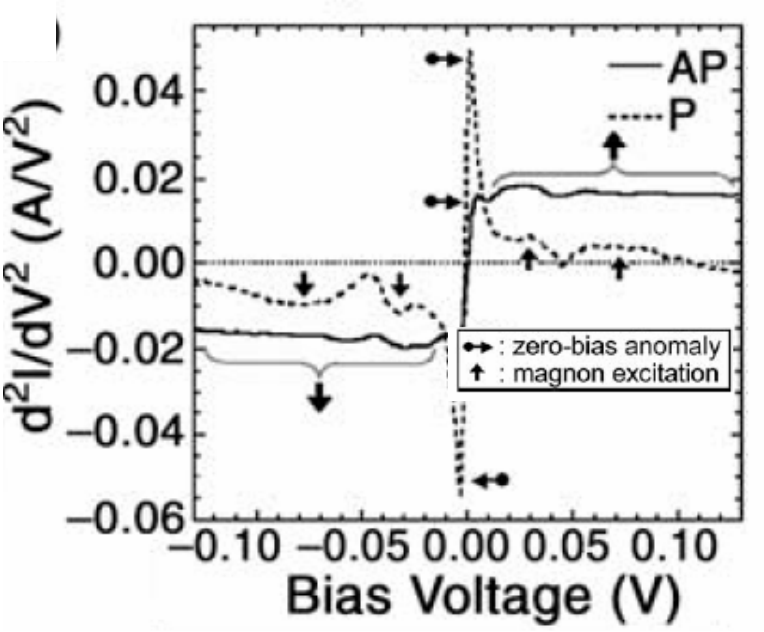


***Fig. 1.8***

*The $d^2I/dV^2$ spectra of CoFeB/MgO/CoFeB MTJ measured at 4.3 K for parallel (P) and antiparallel (AP) states show contributions of inelastic scattering, magnon peaks, adapted from Ref. [37].*

### 1.4. Quantum resonant effect in MgO-based MTJs

The called “coherent tunneling” in the crystalline MgO-based MTJs may contribute to not only very large achieved TMR but also to another quantum phenomena: spin-polarized resonant tunneling. The effect is simply realized by inserting an ultrathin non-magnetic (NM)/ferromagnetic (FM) metal layer between the MgO insulating barrier and one of the two electrodes of a MTJ. Because the conduction electrons can take spin-dependent reflections at the interfaces of the FM and none FM layers and pass through the ultrathin layer via quantum well states as a result of the resonant tunneling (Figure 1.9).[17,18] In a MTJ with the structure of NiFe/Al-O/Cu(001)/Co(001), the tunneling electrons with up-spin and down-spin, which are parallel and antiparallel to the magnetization of the Co electrode respectively, transmit into the Co with different probabilities. For up-spin, it easily transmits into the Co, whereas down-spin has higher probability to be reflected at the Co-Cu interface. If multiple scatterings occur between the Co-Cu and Cu-Al-O interfaces, the electrons with down-spin can form quantum well states (QWs) in the Cu layer. The QWs consequently can be result in oscillations of TMR as functions of the thickness of the NM layer and applied sample bias (Figure 1.10). Since the resonant tunneling via these QWs is perfectly spin-polarized, it is also predicted that the TMR can be enhanced up to about two orders of magnitudes at certain bias voltages corresponding to the QWs energies (Figure 1.11).[21]

However, it is well known that to realize quantum interference in metallic nanostructure is very difficult. Because ultrathin ferromagnetic layers can be in non-uniform structure due to island growth. The island structure leads to the nonuniformity of the ultrathin FM layer as well as large and local distribution of differential conductance *(dI/dV)* spectra which possibly hide the spin-dependent resonant tunneling in average.[40] The improvement in the quality of fabrication processes has led to the development of single crystal MTJs with the ultrathin FM layer; this has been achieved by employing an alternative structure of fully epitaxial Fe(001)/MgO(001)/ultrathin Fe(001)/Cr(001).[41] Although Niizeki *et al.* successfully observed the oscillating component from *dI/dV* spectra at 6 K, it was paint at room temperature (Figure 1.12). It could be mainly due to the large size of junctions and the crystalline quality of the sputter-deposited sample as well as imperfect antiparallel magnetization configuration. This imperfectness is also attributed to the low TMR for MTJs with less than 5 ML Fe. In order to provide clear quantum resonant effect and strong enhancement of TMR at RT, high quality fully epitaxial MTJs with structure of NM/ultrathin FM/I/FM multilayer is necessary.

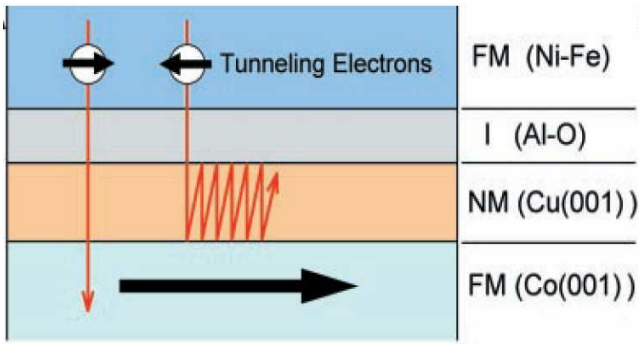


***Fig. 1.9***

*Schematic diagram of the magnetic tunnel junction (MTJ) with FM (Ni-Fe)/I (Al-O)/NM (Cu)/FM (Co) structure shows different tunneling probabilities from the upper to the bottom electrodes for tunneling electrons with different spin directions. FM, NM, and I denote a ferromagnetic electrode, a nonmagnetic layer, and an insulating layer (tunnel barrier), respectively, adapted from Ref. [18].*

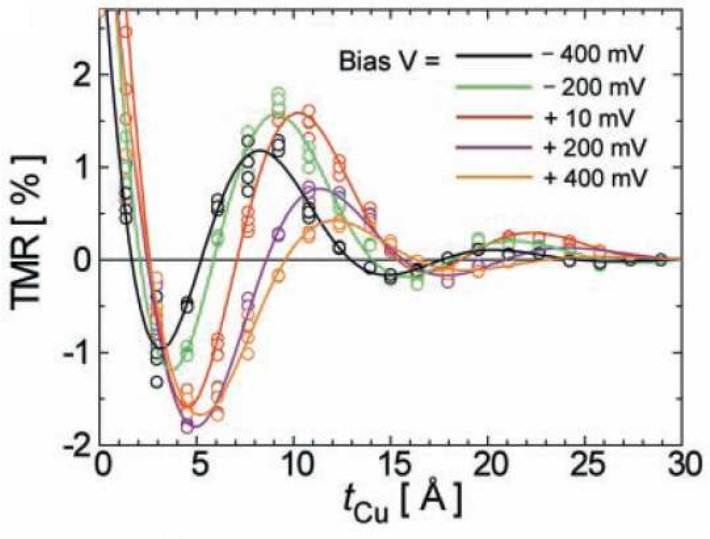


***Fig. 1.10***

*For Co(001)/Cu($t_{Cu}$)/Al-O/$Ni_{80}Fe_{20}$ junctions, oscillations of TMR ratio as a function of the thickness of Cu layers at 2 K and various applied sample biases show different period of Cu thickness, adapted from Ref. [18].*

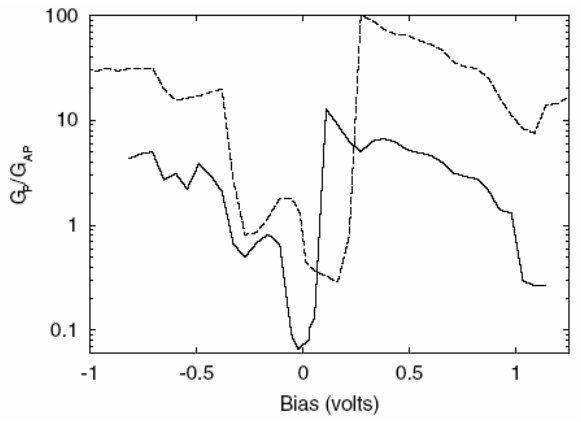


***Fig. 1.11***

*Theoretical calculating conductance ratio as a function of bias voltage shows enhancement peaks for the MTJs with structures of Fe/MgO/FeO/Fe(8 ML)/Cr (solid line) and Co/MgO/Fe(9 ML)/Cr (dashed line), adapted from Ref. [21].*

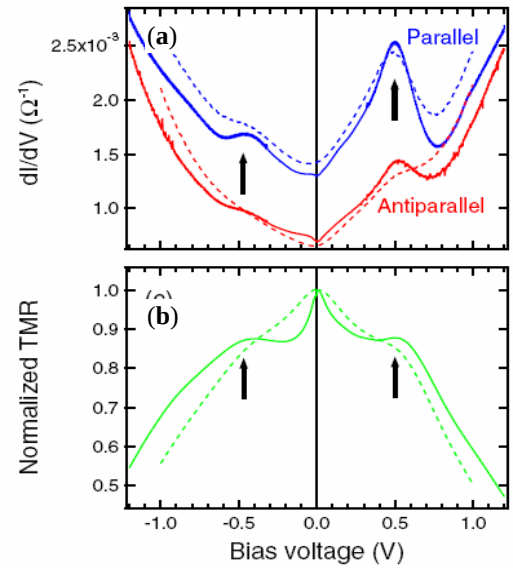


***Fig. 1.12***

*(a) dI/dV spectra, (b) bias voltage dependence of TMR ratio show energy positions of QWs and enhancement of TMR at these energy positions for the MTJ with structure of Cr/Fe(6 ML)/MgO/Fe. The blue (or dark gray) [red (or gray)] lines represent the parallel (antiparallel) magnetization configuration. The solid line (dashed line) represents the data measured at 6 K (RT), adapted from Ref. [41].*

### 1.5. Spin-torque diode effect in MgO-based MTJs

As mentioned in Sec. 1.1, the TMR in crystalline Fe/MgO/Fe tunnel junctions has room-temperature values that can up several hundreds percent. However these values are still much smaller than that of theoretical predicted value of about 1000 %. Experimental results also show a decrease in the TMR as a function of applied bias. Several mechanisms have been proposed to explain these behaviors, such as inelastic spin-flip scattering processes by magnon excitations. On the other hand, the quantum resonant states formed in the ultrathin FM or NM layer of the MTJ have been shown to enhance and control the bias dependence of the TMR. While the TMR effect is conventionally based on the relative orientation of magnetizations affecting the flow of spin-polarized current, Slonczewski and Berger independently predicted a reverse effect.[42,43] Namely, the flow of spin-polarized current in MTJ can transfer spin angular momentum from the carriers to the ferromagnetic and even reverse the orientation of the corresponding magnetization at sufficiently high current density without any applied fields (Figure 1.13). This phenomenon, known as spin-transfer torque, has since been extensively studied both theoretically and experimentally.

The torque also causes the magnetic moment to rotate at potentially useful frequencies and generates a measurable direct-current (*d.c.*) voltage cross the MTJ by applying a small radio-frequency alternating current (*a.c.*). This effect is markedly different from that of a conventional semiconductor diode and was named "spin-torque diode" effect. The spectrum showing a relationship between the generated *d.c.* voltage and the frequency of applied *a.c.* bias was called "spin-diode spectrum". Comparison of the functioning of the semiconductor p-n diode and spin-torque diode is shown in Figure 1.14.[23] For small and uniform oscillation of the magnetic moment, the *d.c.* voltage is given approximately by[23]

$$V_{d.c.} \approx \frac{1}{4}\Delta R \sin^2(\theta) I_{a.c.}^2 \,\mathrm{Re}\left[\frac{if\gamma' ST - \gamma' H_d \gamma' FT}{\left(f_0^2 - f^2\right) - if\alpha\gamma' H_d}\right], \qquad \text{(Eq. 1.4)}$$

where *ST* is the spin-transfer and *FT* is the effective field term, per unit current. γ' is the gyromagnetic ratio (γ' = - γ/2π), $\alpha$ is the Gilbert damping factor, $H_d$ is the demagnetization field perpendicular to the free-layer plane, $f_0$ is the resonant frequency and $f$ is the frequency of the applied alternating current, $I_{a.c.}$.

Besides many potential applications of spin-torque effect such as a microwave oscillator and current-induced switching magnetization, the spin-torque diode also can be used in others future

spintronics devices such as a power detector and amplifier a small electric signal. The spin torque diode effect also provides a quantitative measure of the spin-torque as well as a method to investigate the origin of the spin torque, and to estimate the critical voltage of spin-transfer magnetization switching without applying a large current. To realize the future advantage devices, it must produce a large *d.c.* voltage only in a narrow frequency range around the resonance frequency. It is well known that the maximum *d.c.* voltage produced by spin-transfer is given by[45]

$$V_{d.c.} \approx TMR \frac{V_{r.f.}^2}{V_c} \sqrt{\frac{H_d}{H_c}}, \qquad \text{(Eq. 1.5)}$$

where $V_c$ is the critical voltage required to flip the magnetization. $V_{r.f.}$ if the high-frequency voltage applied to the diode and $H_c$ is the coercivity force. However, to reduce $V_c$ is a challenge of material parameter optimization as well as structure engineering. Large $V_{r.f.}$ causes thermal noise and low power efficiency. To exhibit spin-torque-induced switching and precession, the MgO-based MTJs must have a high TMR and an ultra-low resistance-area (*RA*) product. Such MTJs were originally developed for the read heads of hard disk drives. Then a possibility is that one can improve the TMR by one or two orders by introducing the QWs to the MTJ as discussed in Sec. 1.4. Clarifying the effect of QWs on spin-torque diode properties is therefore important.

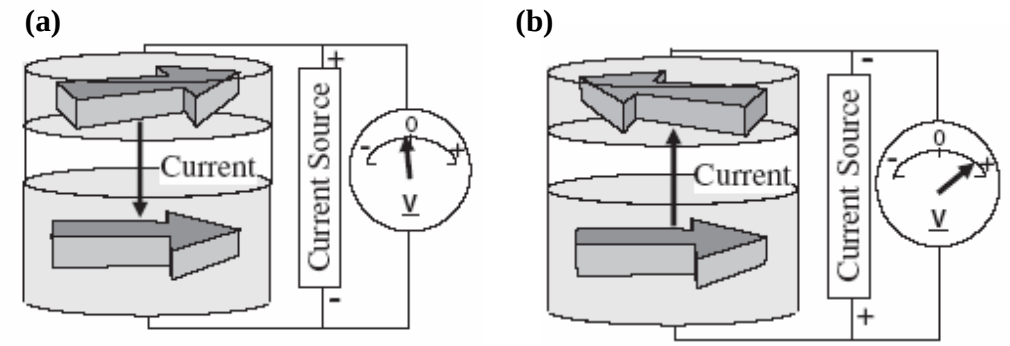


***Fig. 1.14***

*Schematic explanation of the spin-torque diode effect in a MTJ: (a) Applying a negative current that induces a preferential parallel configuration of the spins and small resistance (small negative voltage at given current), (b) applying a positive current which induces preferential antiparallel configuration and high resistance (large positive voltage appearing for a given current). Alternating the current direction at high speed gives rise to a positive voltage on average (rectification function).*

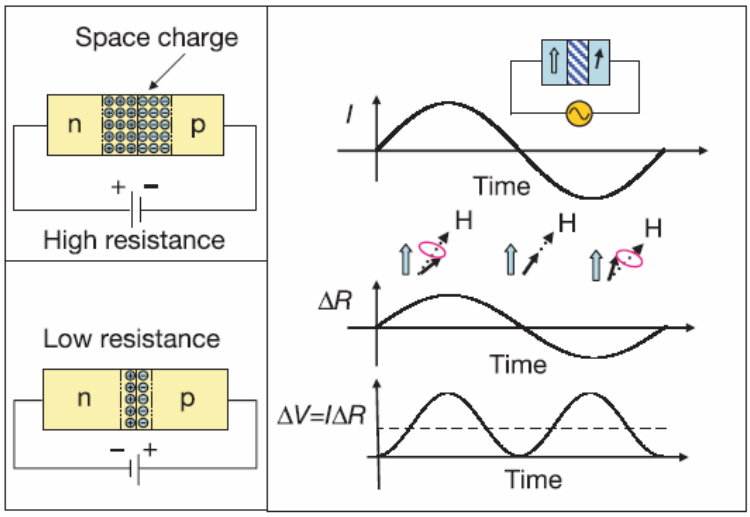


***Fig. 1.15***

*Comparison of the functioning of the semiconductor p–n diode (left panel) and the spin-torque diode (right panel). The difference in resistance during positive and negative currents produces d.c. voltage, in the case of both the diodes, adapted from Ref. [21].*

## 1.6. Purpose of study

### 1.6.1 Study of Kondo and magnon effects in CoFeB/MgO/CoFe textured MTJs

According to Sec. 1.2 and Sec. 1.3, transport properties of sputter deposited MTJs with MgO barrier have been intensively studied since the discovery of giant large tunnel magnetoresistance at room temperature because of their potential applications to magnetoresistive random access memory (MRAM) and coming read heads for ultrahigh density hard disk drives. However, the precise transport mechanism has not been provided a detailed understanding yet. Specially, at regions of low temperature and low bias voltage, and ultrathin magnetic electrode the TMR is suppressed or enhanced due to inelastic scattering effect (magnons), Kondo effect, and quantum resonant tunneling process. In the first part of dissertation, author measured the inelastic tunneling spectra to investigate the transport mechanism and to provide experimental evidence for the observation of Kondo and magnon effects in the MgO-based MTJs.

For Al-O based MTJs, the effect of Kondo scattering on the transport properties have been successfully investigated and providing experimental evidences.[29] At temperature below $T_K$, the low temperature junction resistance is dominated by the Kondo scattering contribution such that the TMR was strongly suppressed. For device applications, crystalline MgO-based MTJs are very important to improve the TMR value. Therefore, it is very crucial to investigate the Kondo effect in MgO-based MTJs, which have a different tunneling mechanism (coherent spin-polarized tunneling mechanism), in order to understand the transport mechanism and also its effect on achievable TMR ratio. In Sec. 3.1.1, author fabricated single crystal MTJs as well as a series of $Co_{60}Fe_{20}B_{20}$/MgO/$Co_{70}Fe_{30}B_x$ MTJs by adding boron with various concentrations ($x$) into top magnetic electrodes to study the influence of metallic-insulator interfaces of these MTJs on the properties of Kondo peaks. Logarithmic temperature dependence in the dynamic resistance of $Co_{60}Fe_{20}B_{20}$/MgO/$Co_{70}Fe_{30}$ MTJ was observed.

In the case of mangnon scattering, one may expect spin-dependent contributions to the electrical conductivity because of the spin-flip scattering of tunneling electrons. Many attempts have been made to find the contribution to the conductivity due to the magnons, excited by tunneling electrons in MgO-based MTJs. It is so far believed that magnon spectra are originated by interface defects, and therefore, strongly depend on the sample quality. In Sec. 3.2, author showed that the magon spectra are rather reproducible among MgO-based MTJs and thus should have intrinsic origins by comparing second derivative conductance spectra ($d^2I/dV^2$) for the

CoFeB/MgO/CoFeB$_x$ MTJs with different boron concentrations. By taking into account magnon density of states, the author will try to provide a consistent explanation of experiment data.

### 1.6.2 Study of quantum resonant effect in fully epitaxial Cr(001)/Fe-wedge(001)/MgO(001)/Fe(001) MTJs

According to Sec. 1.4, it was predicted that the TMR can be enhanced up to about two orders of magnitudes at certain bias voltages due to resonant tunneling via QW states. However, it is well known that establishment of the quantum interference in metallic nanostructure is very difficult, because ultrathin ferromagnetic layers can be in non-uniform structure due to island growth. The island structure leads to the nonuniformity of the ultrathin FM layer as well as large noise of differential conductance (*dI/dV*) spectra which possibly modulate the spin-dependent resonant tunneling. The improvement in the quality of fabrication processes has led to the development of single crystalline MTJs with the ultrathin FM layer. This has been achieved by employing an alternative structure of fully epitaxial Fe(001)/MgO(001)/ultrathin Fe(001)/Cr(001) by using molecular beam epitaxy (MBE) method. In order to provide clear quantum resonant effect and strong enhancement of TMR at RT, the author systematically investigated the spin-dependent resonant tunneling in high quality fully epitaxial MTJs with structure of ultrathin-Fe(001)/MgO(001)/Fe(001) on a crystalline Cr(001) buffer. In Sec. 3.2, the author also successfully provides an evidence of the influence of the thickness of the ultrathin FM layer on quantum resonance energies.

### 1.6.3. Study of spin-torque diode effects in fully epitaxial Cr(001)/Fe-wedge(001)/MgO(001)/Fe(001) MTJs

According to Sec. 1.5, spin-torque diode effect in MgO-based MTJs, exploitation of the spin-transfer torque effect where a spin polarized current passing through a ferromagnetic layer rotates the layer's magnetization is being studied for the development of non-volatile magnetic devices based on current-control. However, in spite of the extensive research in this field the spin-transfer torque effect is not fully understood. Therefore, the author focused on investigating the effect of quantum well states on characteristics magnetization torque in fully epitaxial MgO-based MTJs with an ultrathin-Fe electrode on Cr buffer layer in Sec. 3.3. The author fabricated MTJs with stack structures of ultrathin-Fe/MgO/Fe on Cr buffer layer which was employed as spin-reflection layers by molecular beam epitaxy and e-beam lithography methods. By employing a synthetic antiferromagnet exchange coupling structure of Fe/Cr/Fe the coercivity of the pinned layer could be increased. To observe the QWs and its effects, the electron tunneling spectroscopy spin-transfer torque diode spectra were measured by using conventional lock-in detection technique.

# Chapter 2. EXPERIMENTAL METHOD

All experiments were conducted in the Y. Suzuki, Spintronics Laboratory of Graduate School of Engineering Science, Osaka University except CoFeB/MgO/CoFe samples which were provided by Canon ANELVA Corporation.

## 2.1. Thin film deposition

In this section, first, a brief explanation of fabrication processes for CoFeB/MgO/CoFe sputtering samples is shown. Second, author describes the growth process of the conventional Fe/MgO/Fe MTJs with a wedge-shape MgO(001) tunnel barrier layer. Final, the structure and growth conditions of the MTJs with an ultrathin Fe-wedge layer for studying quantum resonant effect are explained.

*Magnetron sputtering method:*

The MTJs with stack structures of CoFeB(3 nm)/MgO(1.75 nm)/CoFeB(*t* nm)/-CoFe(3-*t* nm) were provided by Canon ANELVA Corporation, where *t* is thickness of the CoFeB inserted-top layer. Fabrication process of the samples is described following. The textured CoFeB/MgO/$CoFeB_x$ multilayer was deposited by a magnetron sputtering (Canon ANELVA C-7100) and subsequently annealed in a magnetic field. Since boron atoms may diffuse easily inside CoFe layer during annealing process (360 $^{o}$C/2 h), difference in *t*, i.e., *t* = 0, 0.03 and 0.3 nm, corresponds to the CoFe, $Co_{69.9}Fe_{29.9}B_{0.2}$ and $Co_{68.6}Fe_{29.4}B_2$ composition of the top ferromagnetic electrode. Details of sample fabrication processes are described in elsewhere.[35]

*Molecular Beam Epitaxy (MBE) method*:

First, a single crystal MgO(001) substrate has been cleaned in acetone and 2-propanol solvents with ultrasonic washing bath to remove contaminants. Then, it was treated under high temperature of 600 $^{o}$C for 30 minutes in high vacuum chamber to remove any adsorbed impurity atoms and molecules. The growth processes of the conventional Fe(001)/MgO(001)-wedge/Fe(001) were basically similar to those of AIST group (AIST: National Institute of Advanced Industrial Science and Technology), which were well described in Ref. [7], except several small changes to adapt to our MBE system. For example, a Co ferromagnetic layer of 200 Å in thickness was grown on the Fe-top electrode instead of sputtering Ir-Mn antiferromagnetic layer to use as a pin layer. Cross-section and reflection high-energy electron diffraction (RHEED) patterns of the MTJ films are shown in Figure 2.1.

To study the quantum resonance effect in MgO-based MTJs with an ultrathin ferromagnetic layer, the MTJs with structures of Au or Cr(001)/Fe(001)-ultrathin/MgO(001)/Fe(001) multilayer were fabricated by MBE method. Here, the crystalline Au or Cr(001) buffer layer is employed as a spin-reflection layer. Because the band structures of Au or Cr are quite different from that of Fe majority spins, thereby providing a large band offset as well as the spin-reflection interface for the majority spins.[44]. Au, Cr, Fe and MgO also have been found to have good lattice matches. It is well known that growth of ultrathin ferromagnetic layer on a nonmagnetic metal layer is a challenge due to mixing, segregation, and island growth. Thus, the growth conditions of the MTJs with the Fe ultrathin layer were changed and detail described following comparing with the growth conditions of the conventional Fe/MgO/Fe MTJ.

In a ultra-high vacuum MBE chamber (less than $5 \times 10^{-8}$ Pa), after depositing a MgO(001) seed layer on the MgO(001) substrate to improve the morphology of the substrate surface, a 500-Å-thickness Au or Cr(001) buffer layer was then deposited at 200 $^{o}$C. The substrate was cooled down to room temperature (RT) and an ultrathin Fe(001)-wedge (thicknesses of from 0 to 10 ML) as a bottom electrode was grown by moving a linear shutter which is parallel to surface of the substrate. The Fe-wedge was then annealed at 300 $^{o}$C to obtain a good crystallinity and flat layer. After cooling down the substrate to RT again, a MgO(001) barrier layer was grown on the Fe(001)-wedge by using a stoichiometric MgO source. The deposited MgO barrier was also annealed at 350 $^{o}$C to improve its crystalline quality. A top Fe-electrode of 40 Å in thickness was deposited and coupled with Cr(10 Å)/Fe(60 Å) to form a synthetic anti-ferromagnetic structure of Fe/Cr/Fe. Cross-section and RHEED patterns of the MTJ films are shown in Fig. 2.2.

It should be noted that a Co layer was used as the pin layer in previous study. However, the Co pin layer has a small coercive force in comparing with that of ultrathin Fe and results in small TMR due to an imperfect antiparallel configuration of bottom and top Fe electrodes. By using a synthetic anti-ferromagnetic exchange coupling Fe/Cr/Fe multilayer with a higher coercive force, the perfect antiparallel configuration and high TMR were observed (see Figure 2.3 for the Au buffer layer samples). Finally, a Au was also deposited as a cap layer of the MTJ films to prevent surface oxidization.

For the study of spin-dependent quantum resonance states effecting on the spin-transfer torque, MTJs with a small resistance and low resistance-area product (*RA*) were fabricated by reducing the thickness of the MgO barrier (1 nm).

In the Fe/MgO/Fe based MTJs, the wedge-shaped MgO or ultrathin Fe layers were grown on the same substrate. Therefore, the dependence of the TMR and dynamic resistances on MgO or ultrathin Fe thicknesses were systematically measured with the negligibly error in thickness between MTJs in the same row.

## 2.2. Sample preparation: Microfabrication

For the studies on Kondo and magnon effects, which are discussed in Sec. 3.1 and Sec. 3.2, the sputter deposited films were patterned into 36 $\mu m^2$ tunnel junctions by high-precision microfabrication techniques (based on electron-beam lithography, a low-damage Ar-ion milling, $SiO_2$ sputtering, and so on). The samples were provided by Canon ANELVA Corporation.

In the case of studies on quantum resonance effect and spin-torque properties in the MTJs with the ultrathin Fe layer, the films were deposited using MBE technique fabricated into tunnel junctions in Osaka University. First, an electron-beam resist (TGMR) was spun on to the multilayer samples and hardened by baking. Then bottom electrodes were patterned using e-beam lithography, with subsequent development to serve as a hard mask, Ar-milling and lift-off processes. Second, the same processes for MTJ cells (size ~ $0.2 \times 0.3$ to $0.2 \times 0.8$ $\mu m^2$) as a rectangular matrix of lines) which was drawn by e-beam lithography in the TGMR resist, were also performed. The wafer with the hard mask was then etched into MTJ stacks using Ar ion beam milling. The films were etched through the top Au electrode, the top Fe/Cr/Fe pin layer, and down to the MgO barrier. The etching depth could be reliably controlled by stopping it at the MgO layer using ion milling probe (IMP-301) based on secondary ion mass spectroscopy system. The entire sample surface is passivated by a sputtered $SiO_2$ of 10 nm thickness an insulator layer. Lift-off process was used to remove $SiO_2$ layer with the TGMR resist and produce contact holes on top of MTJs. Finally, the patterned stacks were capped with Cr/Au double layers which act as the top electrodes. The resulting structure is a large array of 450 MTJs on each substrate (see Fig. 2.4). By using the wedge-shaped ultrathin Fe layer grown on a substrate, the dependences of the MR ratio, conductance on ultrathin Fe thickness ($t_{Fe}$), were systematically measured with the negligible error in $t_{Fe}$ between MTJs in the same row.

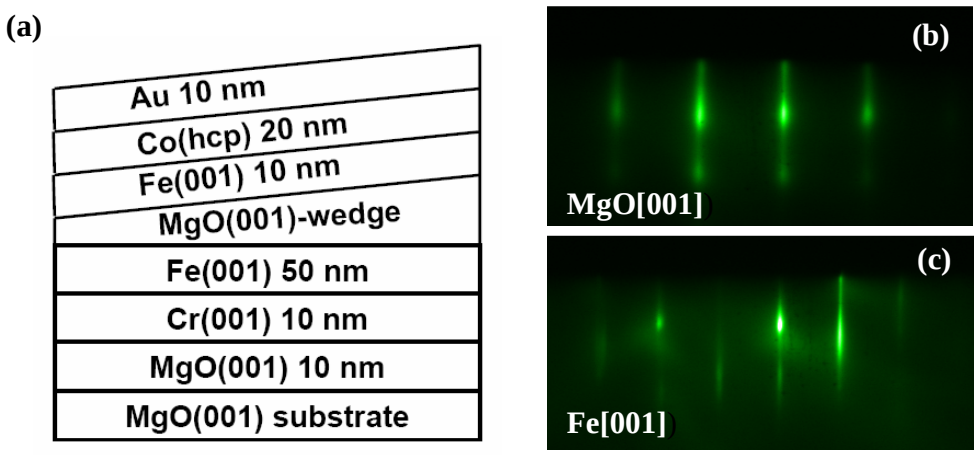


***Fig. 2.1***

*(a). Cross-section of the conventional Fe/MgO/Fe thin films with a MgO-wedge layer. RHEED patterns show high quality of epitaxial films: (b) MgO and (c)Fe in [001] direction.*

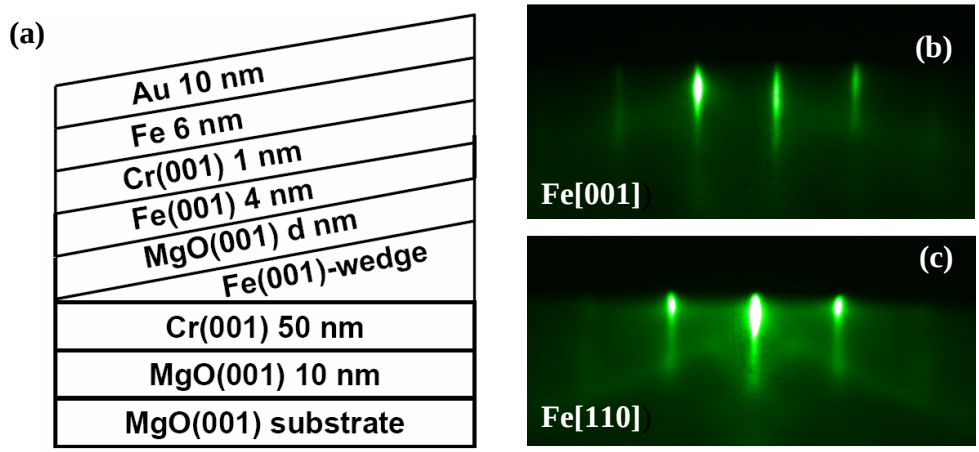


***Fig. 2.2***

*(a). Cross-section of MTJ films with an ultrathin-Fe layer for study the quantum resonance effect. RHEED patterns show high quality of epitaxial ultrathin-Fe film in: (b)[001] and (c) [110] directions.*

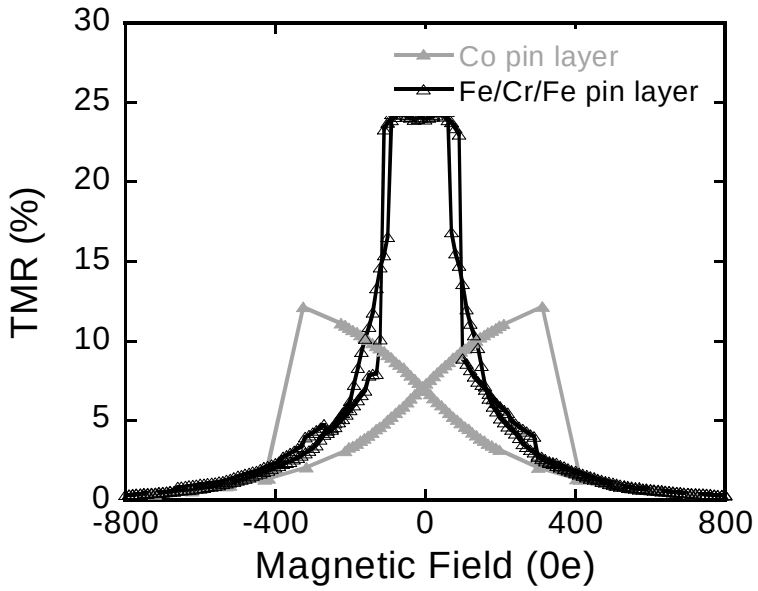


***Fig. 2.3***

*Magnetic dependences of TMR for the MTJs with a Au-buffer, and a Co (gray curve) and synthetic anti-ferromagnetic (SAF) exchange coupling Fe/Cr/Fe multilayer (black curve) pin layers measured at room temperature. The SAF pin layer causes a perfect antiparallel configuration and results in higher TMR.*

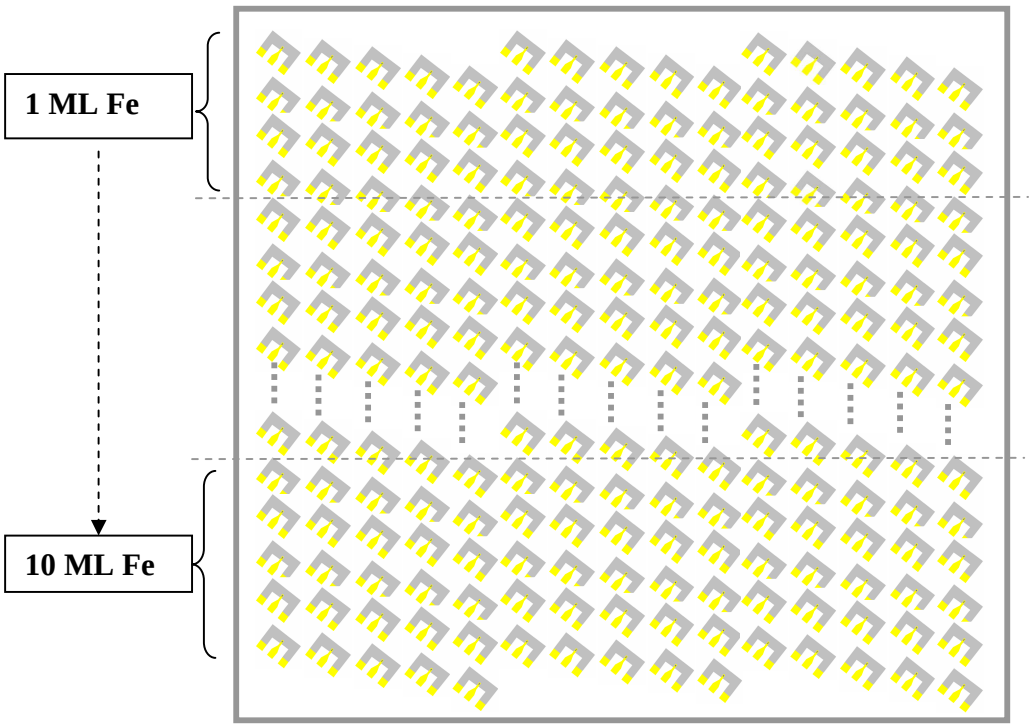


***Fig. 2.4***

*Top-view diagram of all Cr/ultrathin-Fe/MgO/Fe MTJs were fabricated on one substrate. There are 3 MTJs have a same Fe-thickness. From 1 to 10 ML of ultrathin-Fe thickness direction, two neighbor MTJs have a different Fe-thickness by 0.2 ML.*

## 2.3. Measurement methods

In the case of the studies of Sec. 3.1 and Sec. 3.2, the temperature dependences of resistances, and TMR of MTJs were measured with the *d.c.* two- and four-probe methods in Physics Properties Measurement System (PPMS). In those measurements, the samples were attached to PPMS sample holder by using tape and Au wire bonding. The temperature and magnetic field could be systematically or automatically control by Labview programs with high reliability.

To study the dynamic conductance of the MTJs in Sec. 3.1, Sec. 3.2 and Sec. 3.3, the tunneling spectra (i.e. first and second derivative conductance, $dI/dV$ and $d^2I/dV^2I$ as functions of bias voltage) were conducted at various low temperatures and magnetic field in the PPMS system. The tunneling spectrum was well known as a useful method to detect the DOS inside electrodes and also the effects of inelastic scattering processes on conductance with energy resolution down to sub meV. Electric circuits of these measurements are shown in Figure 2.5. For the positive currents, electrons flow from the bottom electrode layer to the top electrode layer. The $dI/dV$ and $d^2I/dV^2$ characteristics also can be derived numerically from data of the *I-V*, and $dI/dV$ respectively.

In Sec. 3.4, the effect of quantum well states on spin-torque properties was investigated by applying an *r.f.* power to MTJs and measuring the *d.c.* voltage that appears across the junction as a consequence of the significant rectification effect of the MTJ (so-called spin-torque diode spectrum).[45] The block diagram of the measurement set up is shown in Figure 2.6.

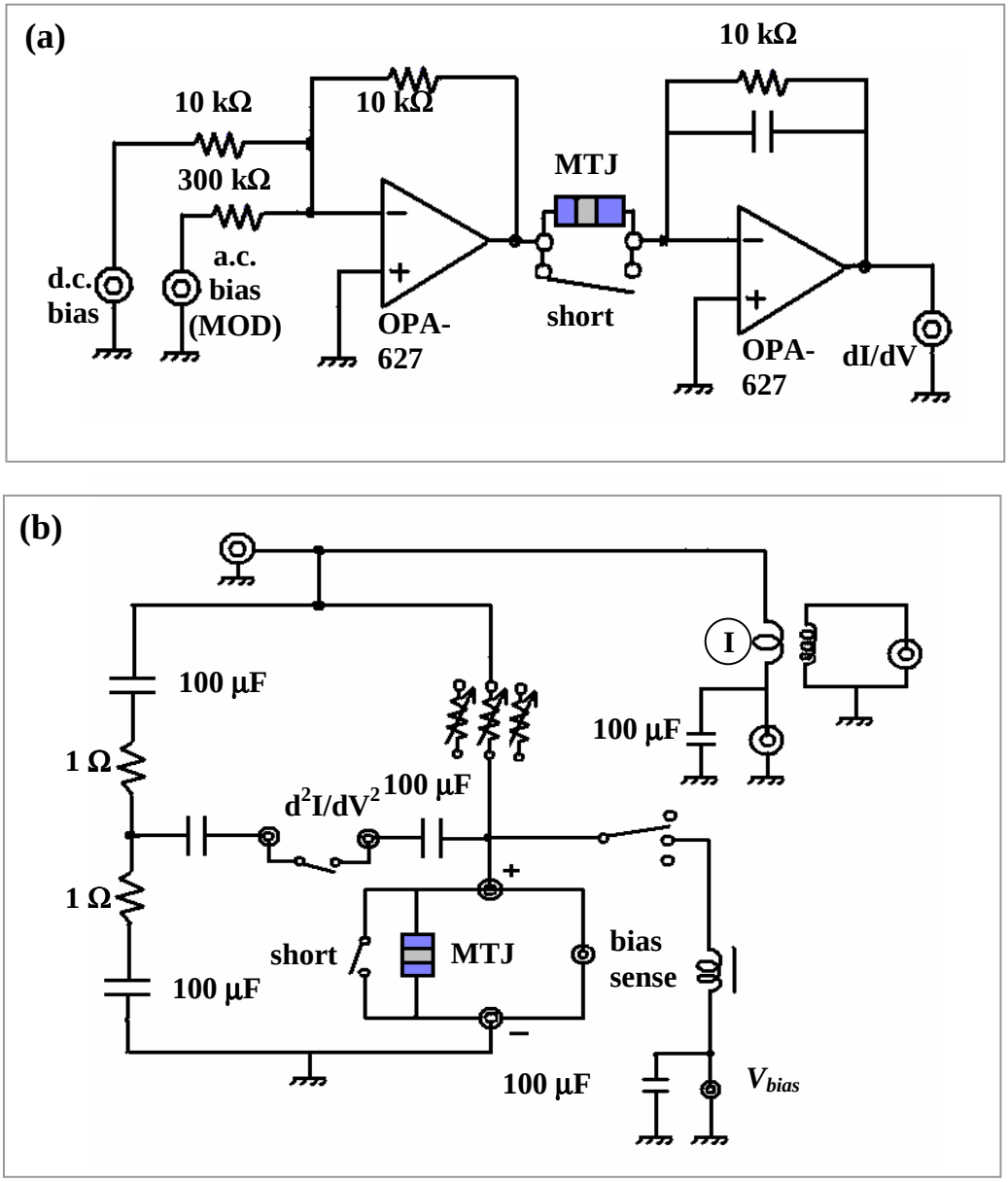


***Fig. 2.5***

*Schematic diagram of electric circuits used for measurements of (a) the dI/dV and (b) $d^2I/dV^2$ characteristics. MTJ, MOD and OPA represent magnetic tunnel junction, modulation and operational amplifier, respectively.*

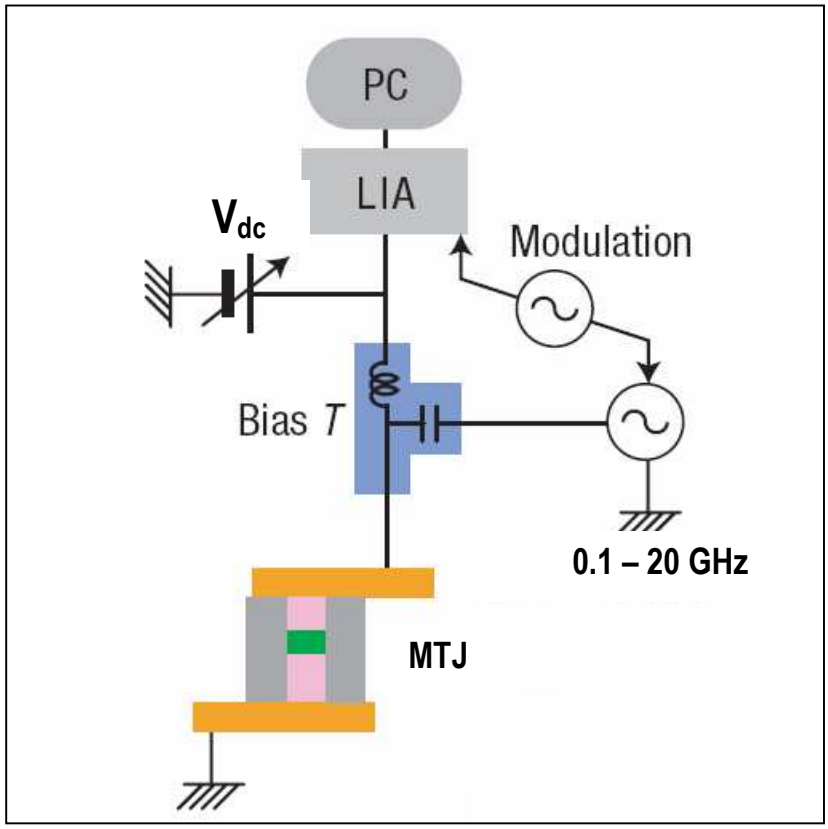


***Fig. 2.6***

*Schematic diagram of electric circuits used for measurements of spin-torque diode spectrum. MTJ, LIA, PC and $V_{d.c}$. represent magnetic tunnel junction, look-in amplifier, personal computer and d.c. bias voltage source, respectively. A bias tee can be viewed as an ideal capacitor that allows a.c. through but blocks the d.c. bias and an ideal inductor that blocks a.c. but allows d.c. The amplitude of high frequency (0.1 - 20 GHz) current is modulated by a low-frequency modulation signal (10 kHz) from LIA and then applied to the MTJ (adapted from Ref. [45]).*

# CHAPTER 3. EXPERIMENTAL RESULTS AND DISCUSSIONS

## 3.1. Kondo effect in MgO-based MTJs

### 3.1.1. The detail of Kondo effect measurement

The MTJs with stack structures included (nanometer) CoFeB(3)/MgO(1.75)-/CoFeB(*t*)/CoFe(*3*-*t*) were provided by Canon ANELVA Corporation, where *t* is thickness of the CoFeB inserted-top layer. In this study, $t$ = 0, 0.03 and 0.3 nm correspond with the CoFe, $Co_{69.9}Fe_{29.9}B_{0.2}$ and $Co_{68.6}Fe_{29.4}B_2$ compositions of the top ferromagnetic electrodes, respectively. The films were patterned into MTJs with a junction size of $3 \times 12$ $\mu m^2$ by using a high-precision micro-fabrication process.

Transport properties, resistance, dynamic conductance, TMR of the MTJs were measured under various conditions of the bias voltage and temperature. The tunneling spectra ($dI/dV$ and $d^2I/dV^2$ as functions of bias $V$) of the MTJs were measured by using the conventional look-in technique for both parallel (P) and antiparallel (AP) magnetization configurations of ferromagnetic electrodes. The voltage modulation was 2 mV. For all spectra, positive bias was considered as the current direction from the bottom CoFeB to the top ($CoFeB_x$) electrode. The schematic measurement system is shown in Figure 3.1.

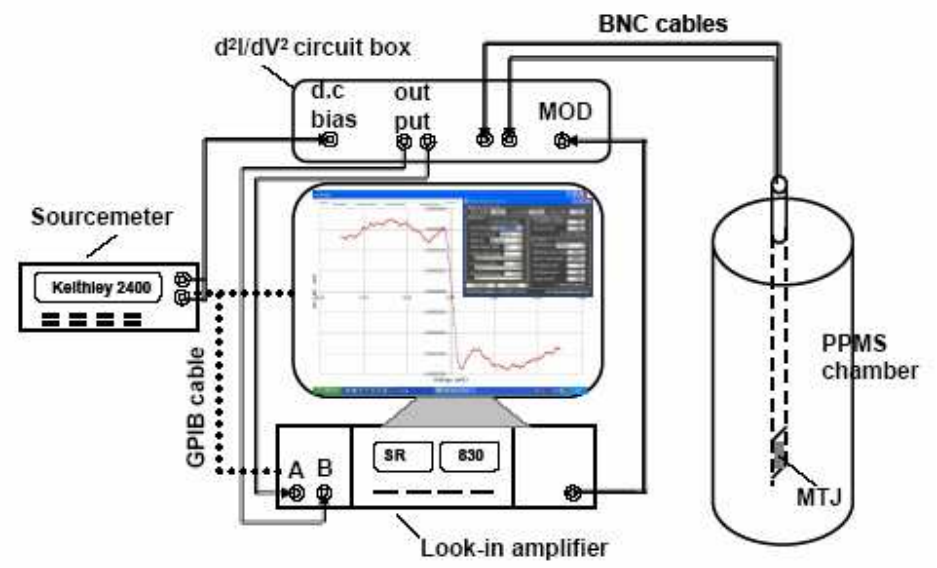


***Fig. 3.1***

*Schematic diagram of equipment setup for measurement of second derivative conductance spectrum by using conventional look-in amplifier technique: magnetic field and low temperature are accurately controlled by programming PPMS system. Arrows show flowing direction of signals.*

### 3.1.2. Kondo effect and Fano interference model

The $d^2I/dV^2$-$V$ characteristics of both P and AP magnetization configurations for the $Co_{60}Fe_{20}B_{20}$/MgO/$Co_{70}Fe_{30}$ MTJ measured at 2 K are shown in Figure 3.2. It should be noted that a difference between the spectra for P and AP configurations is observed. Point symmetrical spectra with respect to the voltage origin were observed as in the case of typical tunnel devices, although the junction structure is not completely symmetrical. It is believed that a weak asymmetry in the spectra is attributed to the difference in the composition and quality of the $Co_{60}Fe_{20}B_{20}$ bottom and $Co_{70}Fe_{30}$ top electrodes of MTJs. The positive bias conveys electrons from the bottom electrode to the top one. The spectrum in the positive bias region, therefore, reflects mainly the unoccupied electronic states in the upper electrode and in the upper electrode-barrier interface.

Around zero bias voltage (4 mV) for both configurations, there are strong peaks which are called “zero-bias anomaly” (ZBA). These ZBA peaks had been attributed to magnetic impurity scatterings, known as the Kondo effect without detailed analysis.[37] Spectra also accompanied by additional peaks such as peak at around ±23 mV (marked as “Mag”) which come from magnon scattering and their characteristics are discussed in Sec. 3.2.

For further investigation of the nature of the ZBA, we performed the detailed temperature-dependent measurements of the ZBA in the second derivative conductance ($d^2I/dV^2$) spectra. The ZBA peaks in the $d^2I/dV^2$ spectra showed a gradual decrease in its intensity and increase in peak energy with increasing temperature (see Figure 3.3).

The ZBA appears as a single dip in the first derivative conductance ($dI/dV$) spectra and are shown in Figure 3.4 for the P configuration, which has less magnon contribution than in the AP case [see discussion in Sec. 3.2]. The dip is deeper and narrower for lower temperature. Above ~100 K, the dip has progressively more parabolic shape reflecting a nonlinear behavior of tunneling conductance assisted by a magnon excitation/annihilation. For all temperatures below ~50 K, the $dI/dV$ curves are nearly identical above ~15 mV and also exhibits a scaling behavior, i.e. the curves at different temperatures have almost identical shapes but with different voltage scales. The width of the anomaly is apparently determined only by thermal broadening. Therefore, the ZBA in the dynamic conductance could suggest that a scattering process was added into electron tunneling processes at the low bias and low temperature regimes. With the

diminution of conductance at the zero bias in our sample, it probably implies that the Kondo effect could be associated with the Fano interference. [46-47]

This effect is a consequence of an interference between the direct electron tunneling and tunneling via magnetic impurity sited in the barrier. The bias dependence of the *dI/dV* spectrum at 2 K was well fitted by the expression (5) in Ref. [46] with the Kondo temperature $T_K$ = 80 K and the Fano parameter $q$ = 0.13.

The Kondo temperature also can be estimated by fitting the temperature dependence of the conductance dip depth as functions of temperature using expression in Eq. 3.1 which was conducted from Refs. [46, 47] for $V$ = 0 (Figure 3.5).

$$\Delta\left(\frac{dI}{dV}\right) \propto (q^2 - f)/(1 - f), \qquad \text{(Eq. 3.1)}$$

and

$$f(T^*) \propto \begin{cases} -\frac{\pi^2}{2}T^{*2}, & T^* << 1 \qquad \text{(Eq. 3.2a)} \\ \left(\ln T^* + \sqrt{\ln^2 T^* + a}\right)/\left(\ln T^* - \sqrt{\ln^2 T^* + a}\right), & T^* >> 1 \qquad \text{(Eq. 3.2b)} \end{cases}$$

where $T^* = T/T_K$ and $a = 3\pi^2/4$.

Taking $q = 0.13$, the Kondo temperature, $T_K \sim 100$ K, was obtained and is in good agreement with that obtained from spectrum shape fitting supporting a validity of the model.

To investigate the origin of the scattering centers, the second derivative conductance spectra measurements were also performed for a series of MTJs with different boron concentrations in the top magnetic electrodes as shown in Figure 3.6. The $d^2I/dV^2$ was normalized to *dI/dV* and represented as $(d^2I/dV^2)/(dI/dV)$ because the intensity becomes independent of the junction resistance and comparison of the intensities of spectra is possible.[37] Overall spectra almost do not depend on the B composition in the top electrodes. The peak position and shapes are almost remained the same, so boron is not the origin of a Kondo scattering. The same measurement for single crystal Fe(001)/MgO(001)/Fe(001) MTJs also performed but it did not show any signals of the Kondo effect (see the inset of Figure 3.6). For the single crystal MTJs, the second derivative conductance spectra are featureless and flat near zero-bias. These results imply that the fully epitaxial Fe/MgO/Fe MTJs have ideal clean interface and barrier and the Kondo effect observed in the sputter deposited MTJs may be caused by magnetic impurities (Fe, Co or Mn) diffused into the MgO barrier through grain boundaries or other defects formed in the textured $Co_{60}Fe_{20}B_{20}$/MgO/$Co_{70-x}Fe_{30-x}B_x$ MTJs during annealing processes.

Oxidized interface between barrier and ferromagnetic electrodes may also result in the Kondo effect with a conductance dip.[31] Although it cannot rule out this possibility, the coherent nature in MgO barrier tunneling may prefer the Fano interference mechanism.

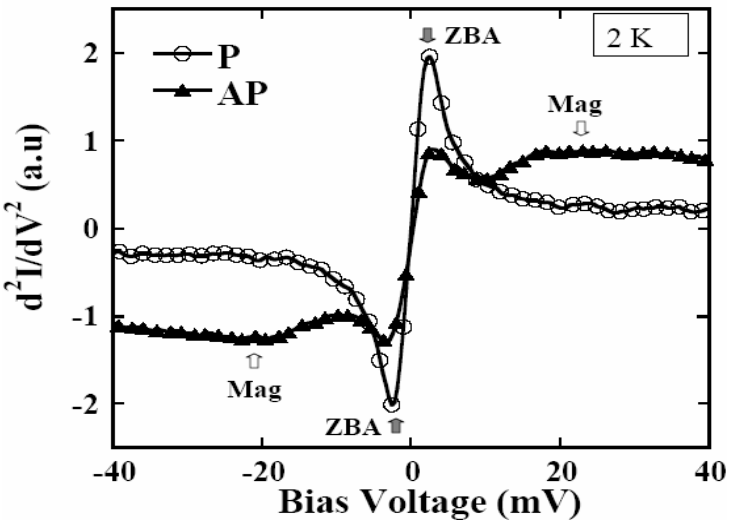


***Fig 3.2***

*$d^2I/dV^2$-V curves of the parallel, P, (open circles) and antiparallel, AP, (solid triangles) magnetization configurations for the $Co_{60}Fe_{20}B_{20}/MgO/Co_{70}Fe_{30}$ MTJ measured at 2 K show the Kondo peaks around zero bias (ZBA). The Kondo peak is sharp and large for P configuration.*

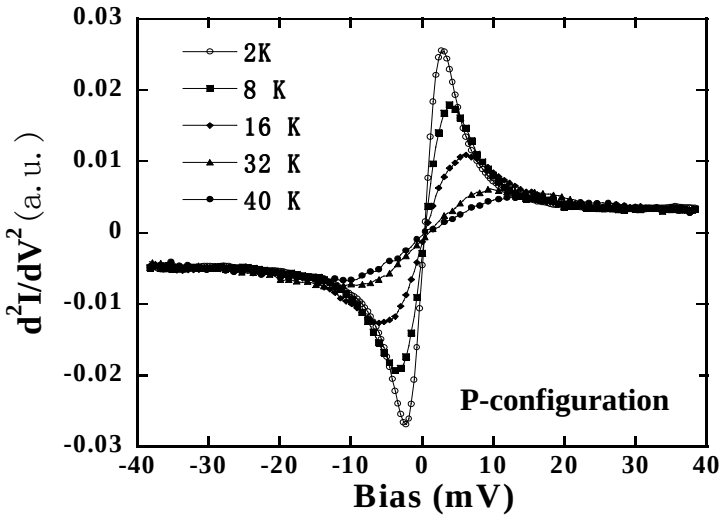


***Fig. 3.3***

*Temperature dependence of the Kondo peak in the second derivative conductance curves measured for parallel configuration at different temperatures: 2 K (open circles), 8 K (solid squares), 16 K (solid rhomboids), 32 K (solid triangles), and 40 K (solid circles). The Kondo peak gradually disappears when temperature increases.*

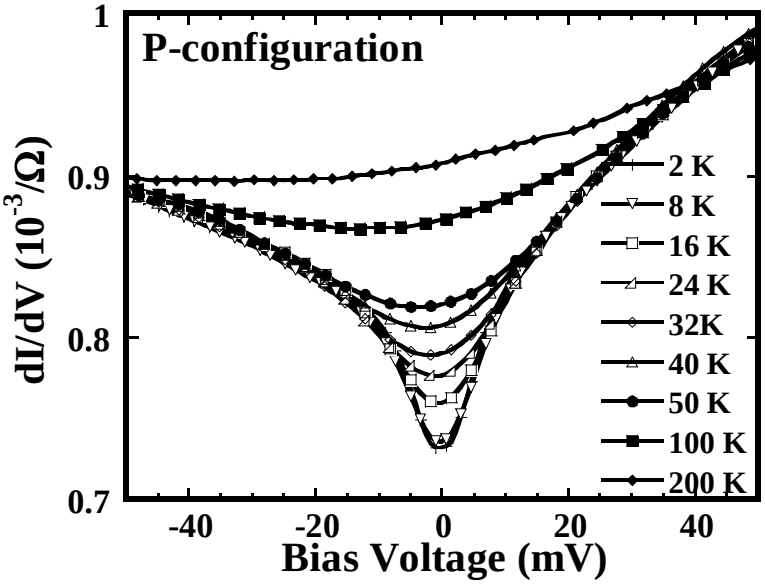


***Fig. 3.4***

*Dynamic conductance-bias curves for the parallel configuration at various temperatures from 2K (bottom curve) to 200 K (top curve): the Kondo effect shows a significant contribution at very low temperature but is eliminated at temperatures higher than 100 K. Kondo temperature was estimated to be about 80 K.*

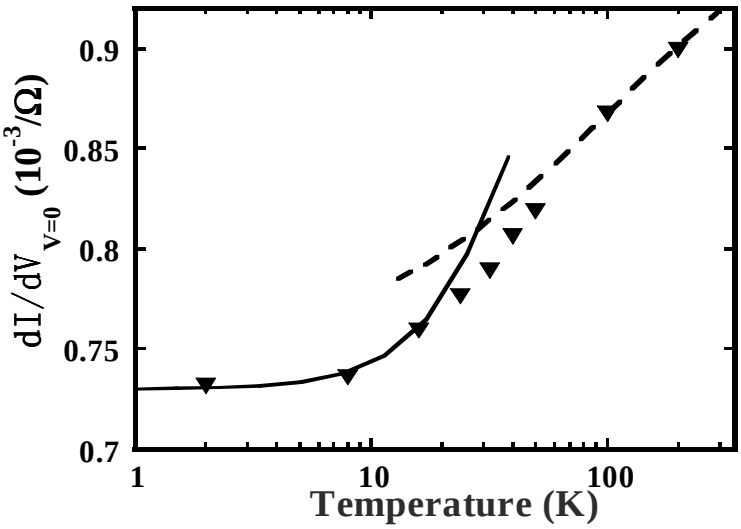


***Fig. 3.5***

*Dynamic conductance at zero-bias (triangles)of MTJ showing a contribution from the Kondo scattering effect. The solid and dash lines are the fitting curves for low and high temperature regimes, respectively. Fitting results show Kondo temperatures about 100 K.*

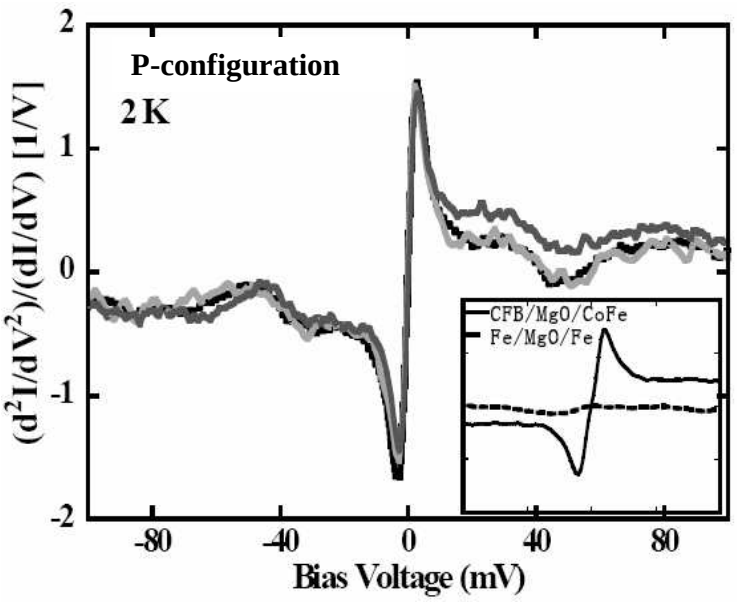


***Fig. 3.6.***

*($d^2I/dV_2$/(dI/dV)-V curves for P configuration of MTJs having $Co_{70}Fe_{30}$, (black thick curves), $Co_{69.9}Fe_{29.9}B_{0.2}$ (grey thin curves) and $Co_{68.6}Fe_{29.4}B_2$ (black thin curves) top electrodes. The inset shows that result of $Co_{60}Fe_{20}B_{20}$/MgO/$Co_{70}Fe_{30}$ (solid curve) and single crystal Fe/MgO/Fe(dotted curve) MTJs. The peak position and amplitude do not depend on B concentration. It means that the changing of B concentrations in top electrode of the MTJs does not effect on contribution of Kondo effect.*

## 3.2. Magnon effect in MgO-based MTJs

### 3.2.1. The details of Magnon effect measurement

To study the magnon effect and its contributions to properties of the MgO-based MTJs, temperature dependences of resistance and TMR were investigated in detail for the same samples which were used in measurements of the tunneling spectrum in Sec. 3.1.

First measurements was performed in a cryostat of Oxford Mag Lab system which uses liquid He to cool down the sample. However, it was difficult to get low temperature less than 4.5 K. It was also difficult to precisely control the temperature that could affect to the analysis of the data because the dimensionality of the magnon dispersion appears in detailed temperature dependence of the conductance. Instead of that the samples were also measured in the PPMS system which can precisely control both magnetic field and temperature. The magnetic fields were set at 0.2 kOe for antiparallel and - 8 kOe for parallel magnetization configurations. The temperature was automatically changed from 2 K to 300 K through 50 temperature points by using a Labview program. A source-meter, Keithley 2400, was used to apply a certain *d.c*. bias voltage/current on the sample. Then a multimeter, Keithley 2100, was used to pickup the drop of current/bias as well as resistance of the sample in the case of 4-probe measurement method.

### 3.2.2. Magnon effect and ferromagnetic scattering impurities

Figure 3.7 shows the $d^2I/dV^2$-$V$ curves of both the P and AP magnetization configurations for the CoFeB/MgO/CoFe MTJ measured at 2 K. Around zero bias voltage (4 mV) for both configurations, there are strong peaks which are called "zero bias anomaly" (ZBA) (see inset of Figure. 3.7). From the strong temperature dependence of this peak,[37] origin of the peak was attributed to a magnetic impurity scattering.[49] The spectra also showed broad peak structure, which extends from ±5 mV to around ±200 mV, accompanied by additional peaks at around ±23 and ±54 mV, and a broad peak at ±85 mV. Below 5 mV, the foot of the broad peak was hidden by the zero bias anomaly peaks. Except for the peak at ±85 mV, the peak intensities were larger for AP configuration than for P configuration.

When a finite positive bias is applied to the MTJs, electrons tunnel into the bottom ferromagnetic layer as hot electrons above the Fermi level $E_F$ for a case of ballistic tunneling.[49] The tunneling electrons may either adsorb magnons and phonons in the host electrode or produce magnons and phonons in the counter electrodes. At the low temperature, however, populations of the magnon and the phonon are low and the adsorption process can be neglected. Therefore, the spectrum for positive bias (negative bias) should relate with the magnon and phonon density of states in top (bottom) magnetic electrode. Since magnon assisted tunneling includes spin-flip process of the tunneling electron, the effect should be pronounced in the AP state while the phonon assisted tunneling should appear in both P and AP states. In our results, the broad peak that extends from 5 to about 200 mV and small peaks at ±23 and ±54 mV are larger for AP configuration; therefore, we attribute origin of these peaks to the magnon assisted tunneling. The broad peak at ±85 mV can be seen in P configuration. In addition, it is reported that the optical phonon in the MgO has its eigen energy at 81 meV.[50] Therefore, we attribute its origin to the phonon assisted tunneling.

A conventional explanation for the magnon contribution to the tunneling current is based on a modeling of the magnon-electron interaction by the *s*-*d* exchange between itinerant *s* and localized *d* electrons.[49] Based on this model, we have calculated the contribution of magnon to the $d^2I/dV^2$ spectrum for MgO based MTJs in which the main part of the current is carried by electrons with normal incidence to the barrier. For this case, we have found that $d^2I/dV^2$ spectra should be simply proportional to the magnon density of state with an abrupt cutoff at maximum magnon energy $E_m$. The maximum magnon energy can be estimated from Curie temperature $T_C$

using $E_m=3k_BT_C/(S+1)$.[49] Employing the Curie temperature of the CoFe and S=3/2, we estimate $E_m$=165 meV. The results roughly agree to our observation that the magnon contribution was significant up to around 200 mV. Although a simple model employed here predicted an abrupt cutoff of the spectrum at high energy edge, it could be smeared since definition of the magnon excitation becomes unclear and it merges with Stoner excitations continuously in such high energy region. The energy position of the low energy peaks (±23 and ±54 mV) agrees with previous observations done for similar MTJs.[49,51] Therefore, one can expect that those peaks have intrinsic origins although the peak energies are much smaller than the expected cutoff energy of the bulk magnon in CoFe. One of the possible origins is the surface magnon. At the surface of the electrode, since coordinate number of the magnetic ions are smaller, they may compose a surface magnon with smaller cutoff energy. Atoms at the atomic step edges may construct 1-dimensional magnons with even smaller cutoff energy. Abrupt and steplike increase in $d^2I/dV^2$ spectrum at very low biasing voltage also agrees to the expected steplike density of states of the surface magnon.

A similar inelastic tunneling process through a NiO barrier has been reported by Tsui *et al.* in Ref. [52]. The observed curves indeed reflect not only one-magnon process but also two and more magnon processes. A possibility that the peak observed at 54 mV in our experiment is a two magnon process should not be neglected, since the observed energy is almost double of the peak at 23 mV. Comparison with neutron scattering and/or Brillouin light scattering is requested to make sure the assignments of the peaks.

The temperature dependences of junction resistance and TMR in a typical CoFe junction are shown in Figure 3.8. The sample shows a TMR of 152% at RT, increasing to 236% if it is cooled to 2 K. This is a relative increase of 64%, while at the same time the sample resistance changes 4% and 78% in P and AP configurations, respectively. Compared to the Al-O barrier junctions, the change in resistance in P case is much smaller than that of AP case. We tried to fit the temperature dependence of the conductance in AP state, $1/R_{AP}(T, V\approx0)$ by assuming both surface magnon absorption (two-dimensional (2D)) and bulk magnon absorption (three-dimensional (3D)) in the following expression:[49,53]

$$\left(\frac{1}{R_{AP}(T)}-\frac{1}{R_{AP}(0)}\right)\propto\begin{cases}-kT\ln\left(1-e^{\frac{-E_C}{kT}}\right), & \text{(Eq. 3.3a)}\\ kT^{\frac{3}{2}}. & \text{(Eq. 3.3b)}\end{cases}$$

here, $E_c$ is a magnon gap. $E_c$ may arise because of a cut in the wavelength of the surface magnon or a surface magnetic anisotropy. As shown in a linear scale graph (the inset of Fig. 3.8) if we employ $R_{AP}(0)$=163.59 Ω, both 2D and 3D magnons give good fittings to the experimental data. The obtained fitting parameter of $E_c$ is 1.1 meV for 2D. The $E_c$ of 2D magnon is in good agreement with the results of Drewello *et al.*, [39]. It also should be noted that in Ref. [53] only obtained a good fitting of temperature dependence of experimental $R_{AP}$ in high temperature region but not in low temperature region less than 50 K. These results and the abrupt increase in the second derivative conductance at very low biasing voltage reflecting the steplike density of states of the spin waves suggest that the surface magnons play an important role in our samples.

To evaluate the effect of magnon contribution to spin-dependent transport property of MTJs with different B concentration in the CoFe top electrode, a comparison of the $d^2I/dV^2$ spectrum in these MTJs was systematically carried out. We normalized the $d^2I/dV^2$ to $dI/dV$ represented as $(d^2I/dV^2)/(dI/dV)$ because the intensity becomes independent of the junction resistance and comparison of the intensities of spectra is possible.[52] Overall shape and intensity of the normalized $(d^2I/dV^2)/(dI/dV)$ spectra for P configuration almost did not depend on the B composition of the top electrodes (not shown) while a considerable difference was observed for those of AP configuration as shown in Figure 3.9. In AP configuration, the intensity of the $d^2I/dV^2$ spectra is systematically reduced from MTJ without boron to 2 % of boron inclusion. The peak positions and shapes were remained the same. This result shows that the B inclusion has only negligible contribution to a nonmagnetic part of the $d^2I/dV^2$ spectrum but significant effect on the magnetic part. A systematic change was also observed in the TMR ratio (Figure 3.10). TMR ratio was 226% at 4.2K and was largest for the MTJ without boron. The MTJ of $Co_{69.9}Fe_{29.9}B_{0.2}$ electrode shows a middle TMR ratio of 203 %. The MTJ of $Co_{68.6}Fe_{29.4}B_2$ top electrode shows a lowest TMR of 66.1 %. Therefore, it can be concluded that inclusion of the boron did not show significant modification in magnon dispersion but it affected on the spin polarization of the tunneling electrons. Then, a change in the TMR ratio resulted in relative significance of the magnon assisted spin-flip process to the conduction. Therefore, spectrum intensity was changed. The addition of B may result in a reduced $T_C$ of the ferromagnetic electrodes and, consequently, should reduce the energy of excited magnons. However, such changes were not observed in our experiment. This result proposes a negligible change in the exchange constant by an inclusion of such small amount of boron atoms.

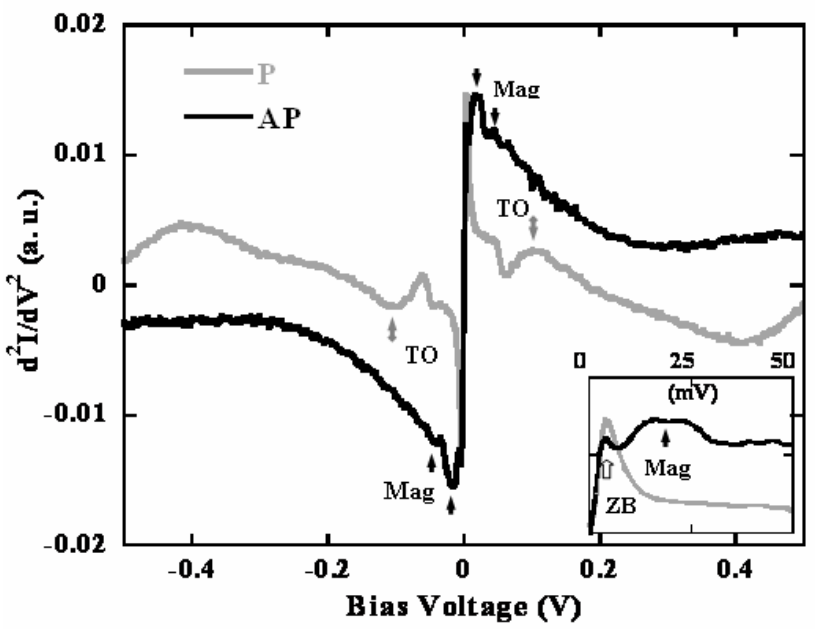


***Fig. 3.7***

*$d^2I/dV^2$-V curves of the P (gray curve) and AP (black curve) magnetization configurations for the CoFeB/MgO/CoFe MTJ measured at 2K. The inset shows the spectra in low bias region. Arrows with "ZB," "Mag," and "TO" are stand for zero-bias anomaly, excited magnon, and transverse optical phonon (Ref. [50]) contribution peaks, respectively. The magnon peaks are observed at around 40 mV and dominate for AP configuration.*

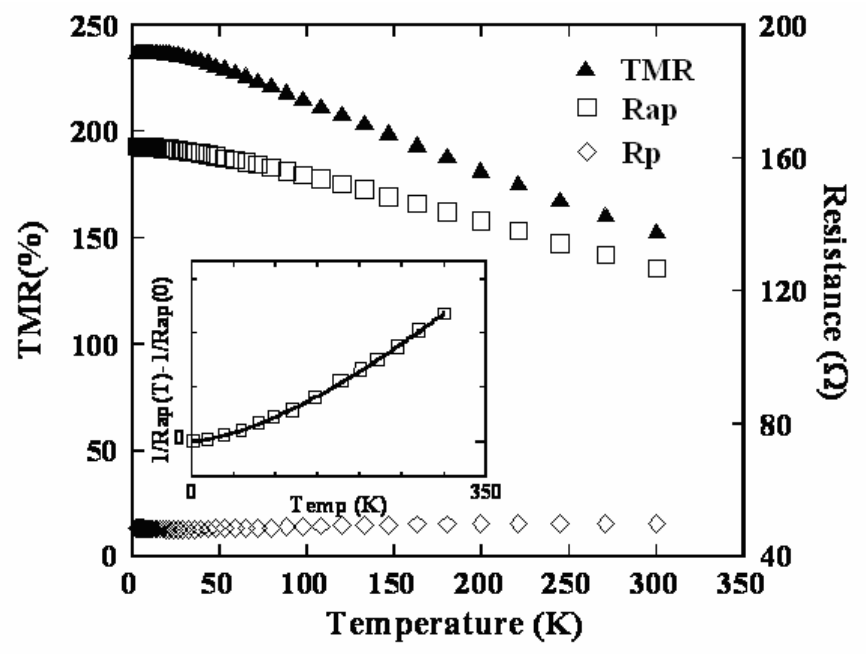


***Fig. 3.8***

*Temperature dependence of resistance (R = V/I, I = 50 μA) for the parallel (open circles) and antiparallel (open squares) configurations and TMR (solid triangle) for the MTJ having CoFe electrode. Inset figure: black lines are the fitting for 2D and 3D models (see the text). The magnon scattering is contributed to a reduction of TMR at high temperatures.*

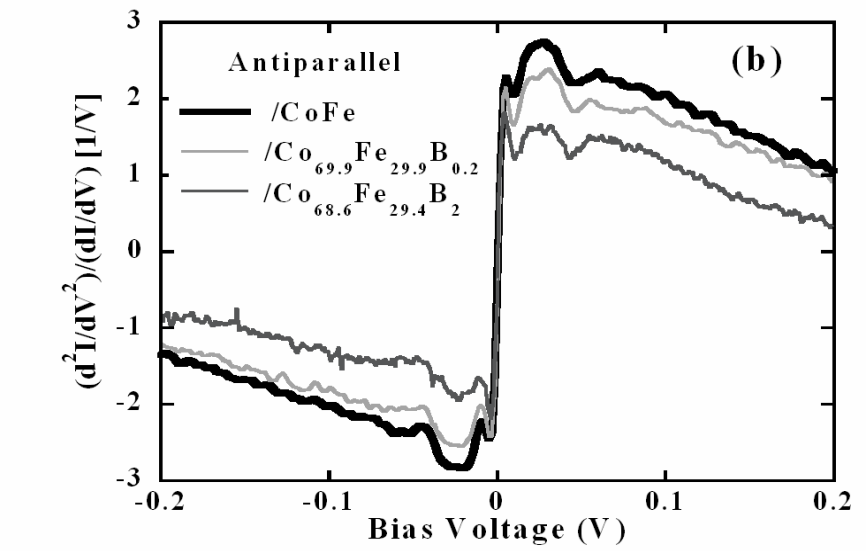


***Fig. 3.9***

*$(d^2I/dV^2)/(dI/dV)$ as a function of bias voltage for AP configuration of MTJs having CoFe (black thick curve), $Co_{69.9}Fe_{29.9}B_{0.2}$ (gray thin curve), and $Co_{68.4}Fe_{29.6}B_2$ (black thin curve) top electrodes measured at 2 K. The peak position reflecting magnon dispersion is not effected by the added boron concentration. The spectrum intensity was reduced by B inclusion.*

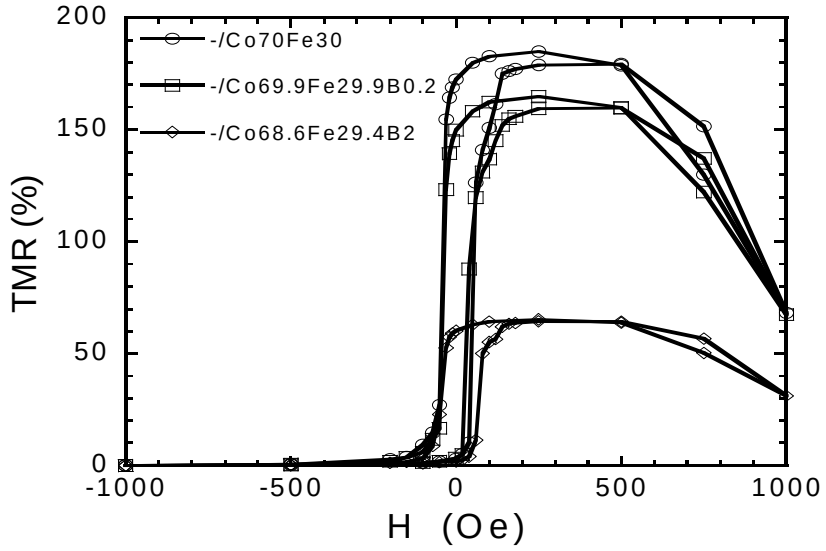


***Fig. 3.10***

*Magnetoresistive hysteresis loop of MTJs with different top electrodes: $Co_{70}Fe_{30}$ (circles), $Co_{69.9}Fe_{29.9}B_{0.2}$ (squares), and $Co_{68.6}Fe_{29.4}B_2$ (rhomboids). Increasing B concentration is contributed to change spin polarization of the tunneling electrons as well as the TMR.*

## 3.3. Quantum resonant effect in epitaxial MTJs

### 3.3.1. The detail of quantum resonant effect measurement

High quality fully epitaxial Fe(001)/MgO(001)/Fe(001) film with wedge-shaped ultrathin MgO and Fe layers were fabricated by using molecular-beam epitaxy (MBE) method. The MTJ films were patterned into MTJs with several kinds of junction areas of $0.2 \times 0.5 \sim 3 \times 10\ \mu m^2$. Because the wedge-shaped ultrathin MgO or Fe layer was grown on the same substrate, the dependences of the MR ratio, conductance on ultrathin MgO/Fe thickness ($t_{Fe}$), were systematically measured with the negligible error in thickness between MTJs in the same row.

To detect the quantum interference effect in the MTJs, we measured the thickness dependences of transport properties such as TMR, resistance-area (RA) product for the MTJ with the MgO-wedge layer. For the MTJ with the ultrathin-Fe wedge layer, bias dependence of the differential conductivity (*dI/dV* spectrum) was measured by using the conventional look-in technique. Positive bias voltage was considered as the current direction from bottom ultrathin Fe to the top Fe electrode.

### 3.3.2. Oscillatory magnetoresistance in epitaxial MTJs with a MgO-wedge barrier

A fully epitaxial Fe/MgO/Fe MTJ exhibits some interesting phenomena such as an intrinsic interlayer exchange coupling mediated by spin-polarized tunneling electrons. Moreover, one of the most interesting phenomena observed in this MTJ is a TMR oscillates as a function of tunneling barrier thickness ($t_{MgO}$). This behavior can help us deeply understanding the tunneling mechanism, coherence tunneling, of the Fe/MgO/Fe. The TMR oscillation has studied both in theory and experiment.[5,7] In the Ref. [7], Yuasa *et al*. showed high TMR and clear oscillation of TMR and it could be considered as a standard quality of the epitaxial Fe/MgO/Fe MTJ. For further study of quantum resonance effect in the Fe/MgO/Fe MTJ with an ultrathin-Fe, author has tried to fabricate the MTJ which somehow has high quality as that of Ref. [7]. Because it was necessary to investigate the fabrication conditions of a new MBE system and find out the optimum conditions. Finally, author could make the MTJ with TMR of 200% at room temperature. An oscillatory barrier thickness dependence of TMR was also observed as shown in Figure 3.11. According to Ref. [5], it is an evidence of existing quantum interference effect in the MTJ. To explain this behavior an interference between tunneling states proposed by Butler *et al.* as it is briefly described as follows. In MgO, two evanescent states that correspond to $\Delta_1$ and $\Delta_5$ at $k_{//} = 0$ have complex wave vector as $k_1 = k_1^r + iK_1$ and $k_2 = k_2^r + iK_2$, respectively. When $k_{//} \cdot \Delta z > 0.59$ ($\Delta z$ is the interlayer spacing of MgO(001)), none zero real parts of the complex wave vectors $k_1^r \neq k_2^r$ ($\neq 0$) and $K_1 = K_2 = K$, these states could cause an oscillation of tunneling transmittance as function of $t_{MgO}$ as the following expression:[7]

$$\begin{aligned} T &= \left|\exp\left(ik_1.t_{MgO}\right) + \exp\left(ik_2.t_{MgO}\right)\right|^2 \\ &= 2\exp(-2K.t_{MgO}).\left\{1+\cos\left(\left(k_1^r - k_2^r\right).t_{MgO}\right)\right\} \end{aligned} \qquad \text{(Eq. 3.4)}$$

The tunneling transmittance for a given $k_{//}$ thus oscillates as a function of $t_{MgO}$ with a period of $2\pi/(k_1^r - k_2^r)$. This transmittance oscillation can be an origin of the observed oscillation of the TMR with respect to $t_{MgO}$. Recently, Matsumoto et al. had reported the TMR oscillation as a single-period of 3.17 Å oscillation function plus a back ground curve for the epitaxial Fe/MgO/Fe MTJ.[54]

The size of TMR effect in the epitaxial Fe/MgO/Fe MTJs grown at Osaka University is shown in Fig. 3.11 as a function of $t_{MgO}$ (open circles). Then a background curve (dashed line in Fig. 3.11) approximated by a quadratic function TMR curve was subtracted. The result is shown

in Figure 3.12. The subtracted data points were again fitted by a simple cosine curve with an oscillation period of 3.5 Å. However, there is a small discrepancy in comparison with the Matsumoto *et al.* result. A possible reason is that there are some scattered values for thinner MgO regime which could be attributed to a scattering of the etching depth into the MgO-wedge barrier. It was found that if the sample is etched over the MgO barrier the TMR would become worse with much lower TMR in comparison with the case of etching depth stopping just at the middle of the MgO barrier. Its reasons were not clear identified but it was a systematical error of fabrication technique.

The obtained high TMR as well as high quality MTJ opened a further study on quantum resonant states by introducing an ultrathin-Fe layer between the MgO barrier and a crystalline Cr(001) buffer which is employed as a spin-reflection layer. The details of that study are discussed in next sections.

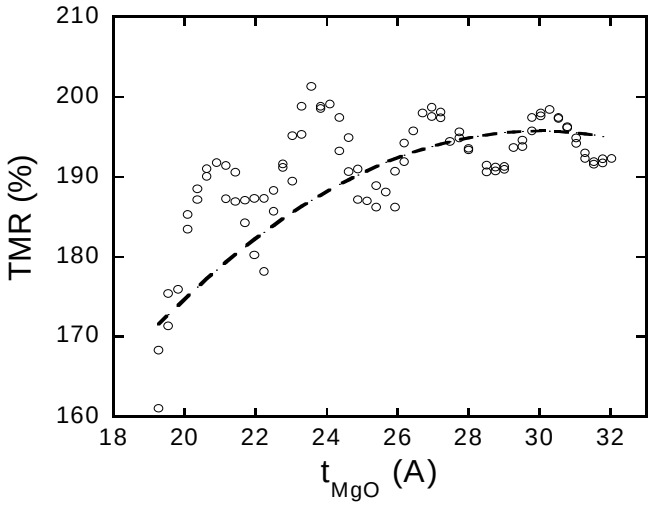


***Fig. 3.11***

*MgO thickness dependence of TMR for epitaxial Fe(001)/MgO(001)/Fe(001) MTJs at room temperature. Dashed line represents a background curve, which is approximated using a quadratic function.*

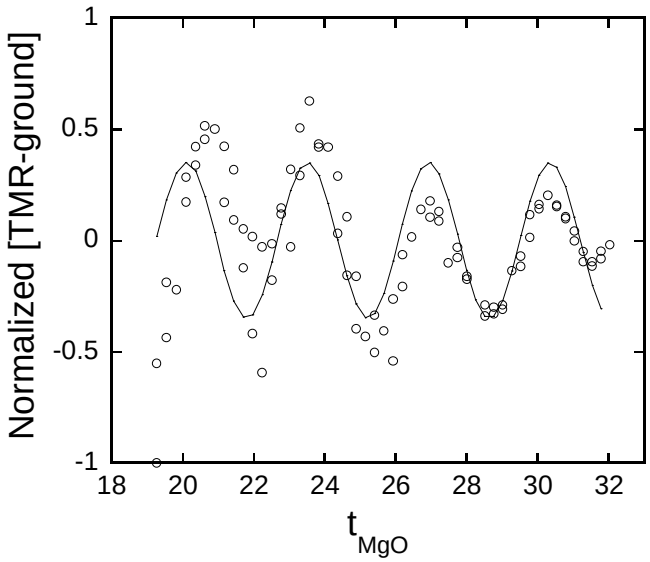


***Fig. 3.12***

*Oscillatory component of TMR (after a subtraction of a quadratic background) as a function of $t_{MgO}$ for epitaxial Fe(001)/MgO(001)/Fe(001) MTJs at room temperature. Solid line is the fitting curve with a single period of 3.5 Å.*

### 3.3.3. Ultrathin Fe thickness dependence of quantum resonant energies

The improvement in the quality of fabrication processes has led to the development of MTJs with the ultrathin FM layer; this has been achieved by employing an alternative structure of fully epitaxial Cr(001)/ultrathin-Fe(001)/MgO(001)/Fe(001) as reported in a recently study using sputtering method.[41] Although it was only successful in observing a clear oscillating component in *dI/dV* spectra at quite low temperature. In my study, the epitaxy technique was used to grow the films of MTJs. The quality of films was significantly improved as well as TMR and clear quantum interference effect was observed at room temperature.

I achieved very high TMR ratios of about 130% and 90% at room temperature for single crystal Fe/MgO(20Å)/Fe MTJs with ultrathin Fe thickness of 10 and 5 ML, respectively (see the inset of Figure 3.13). Moreover, magnetoresistance curves of the MTJs showed a nearly complete antiparallel magnetization configuration even in the case of the ultrathin-Fe layer if it is thicker than 4 ML. These results suggest that quality of the samples is much improved by using molecular beam epitaxy technique. For all MTJs, thickness dependence of TMR at room temperature is plotted and shown in Figure 3.13. Using the same analysis process that was used for a case of the MgO-barrier thickness dependence of TMR, the background was fitted by a quadratic function (solid line in Figure 3.13) and subtracted. The subtracted function data points are shown in Figure 3.14 as a function of the Fe layer thickness. The data are fitted by a single oscillatory curve with a period of about 2.2 ML. However, there are scattered data points around the fitting curve. Especially, below 4 ML very low TMR could be attributed to an incomplete AP alignment of the magnetization that was observed in TMR hysteresis loop of the MTJ with the ultrathin-Fe electrode. The oscillation with 2 MLs period could have its origin in the interference between incoming states and reflecting states inside an ultrathin Fe electrode. Such very short period should only be observed for the sample with precise layer-by-layer epitaxial growth of Fe(001).

To avoid the effect of the imperfect antiparallel configuration, author had tried to plot the thickness dependence of parallel state conductance as shown in Figure 3.15. Observation of conductance oscillation with respect to the Fe-wedge thickness was obtained for the first time. By subtracting the background using a linear function (represented by solid line in Figure 3.15), the subtracted data were again plotted in Figure 3.16 and fitted well by a single-period oscillation function (solid curve). Fitting parameter of the oscillatory period is 2 ML. It could be noted that

the oscillations of TMR and parallel conductance have the same period of about 2 ML. Therefore, this oscillation should be attributed to the interference of coming and reflecting electrons inside the ultrathin-Fe electrode, and it is different from the origin of the TMR oscillation with respect to the MgO-barrier thickness. Clarifying the mechanism of that oscillatory tunneling transmittance with respect to the ultrathin Fe thickness will provide deeper understanding of the tunneling mechanism in the MgO-based MTJs.

The bias dependence of the first derivative conductance in MTJs with a MgO barrier thickness of 20 Å and different Fe electrode thickness are shown in Figure 3.17 for the parallel magnetization. Here, it is well known that the *dI/dV* spectrum should correspond to the features of the unoccupied density of states in a electrode of the MTJ.[55] A clear oscillation component emerged on a parabolic-like background spectrum was observed for MTJs with ultrathin Fe electrodes even at RT. As we defined a positive bias voltage as electrons flow from the ultrathin Fe electrode to the Fe top electrode, and vice versa, a clear oscillation of the conductance for the negative bias should be attributed to quantum resonant effect in the unoccupied states in the ultrathin Fe electrode. It should be noted that other first derivative conductance spectra for MTJs having different layer structures of Cr/MgO/Fe and conventional Fe/MgO/Fe do not show any signal of quantum resonant peak as it is shown in Figure 3.18. The MTJs with the structure of Fe/MgO/Fe grown on Cr(001) buffer shows a similar behavior with that of the conventional Fe/MgO/Fe that is directly grown on MgO substrate. The MTJ with the structure of Cr/MgO/Fe shows an asymmetry in bias direction due to different interfaces. These observations can provide evidences of quantum well states formed in the ultrathin Fe electrodes.[57,58] The clear oscillations of the dynamic conductance with respect to the bias voltage were also observed for the MTJs with different MgO-barrier thicknesses of 13 and 18 Å (not shown). The resonant peak positions which correspond to the local maxima of the DOS move systematically to higher bias for thinner ultrathin Fe electrodes in all MTJs and are independent of the MgO-barrier thickness as shown in Figure 3.19. We also note that a QW state appeared in each monolayer thickness as Nagahama *et al.* reported in Ref. [59]. However, a theoretical calculation of Lu *et al.* in Ref [21] showed that the resonances do not occur for every layer thickness. A possible reason for the difference between experimental and theoretical data is that Lu *et al.*, had introduced a FeO layer on the interface to his calculations. The FeO layer modifies DOS at interface and consequently can result in different current-voltage characteristics.[60] In addition, Theodonis *et al.*, predicted that the QW states can be observed for every atomic layers in an ideal double-barrier MTJ

consisting of FM/I/FM($N_c$)/I/FM structure, where FM, I and $N_c$ represent for ferromagnetic metal, insulator layers and number of atomic layers, respectively. [61] If we consider to such a high TMR of 130% for the MTJ with an ultrathin Fe electrode of 10 MLs, it probably indicates that the MTJ had a high quality interface without FeO layer. In figure 3.19(a), theoretically predicted QWs positions [21] are shown as red triangles.

To investigate a deviation between my experimental results and *ab-initio* calculation done by Lu *et al.*, I have calculated *dI/dV* peak position using very simple equation

$$\boldsymbol{k}_{\boldsymbol{Fe},\uparrow}\left(\bar{\Gamma}\right)\boldsymbol{d}_{\boldsymbol{Fe}} + \Delta\boldsymbol{\varphi}_{\boldsymbol{Fe},\boldsymbol{MgO}} + \Delta\boldsymbol{\varphi}_{\boldsymbol{Fe},\boldsymbol{Cr}} = \boldsymbol{2n\pi} \qquad \text{(Eq. 3.5)}$$

where $d_{Fe}$ is the Fe layer thickness. $\boldsymbol{k}_{\boldsymbol{Fe},\uparrow}\left(\bar{\Gamma}\right)$ is the wave vector of Fe majority $\Delta_1$ band at $\bar{\Gamma}$-point. $\Delta\varphi_{Fe,\,MgO}$ and $\Delta\varphi_{Fe,\,Cr}$ are phase shifts by reflections at Fe/MgO and Fe/Cr interfaces, respectively. n is an integer number. Using the $\boldsymbol{k}_{\boldsymbol{Fe},\uparrow}$ taken from band calculation for bulk Fe and taking $\Delta\boldsymbol{\varphi}_{\boldsymbol{Fe},\boldsymbol{MgO}} + \Delta\boldsymbol{\varphi}_{\boldsymbol{Fe},\boldsymbol{Cr}}$ as a fitting parameter, I got QWs position map as shown in Fig. 3.19(b). Surprisingly, a fitting using single parameter, $\Delta\boldsymbol{\varphi}_{\boldsymbol{Fe},\boldsymbol{MgO}} + \Delta\boldsymbol{\varphi}_{\boldsymbol{Fe},\boldsymbol{Cr}} = \boldsymbol{0.1[rad]}$ (energy dependence is neglected), provides fairly nice agreement with the experimental results. Observed disagreement with *ab-initio* calculation may cause on the different phase shift at interface with oxidized layer employed in the theory.

Also, we observed clear quantum oscillations of the differential TMR in the samples as shown in Figure 3.20. The TMR were clearly modulated at the bias voltages corresponding to the resonant peaks. The amplitude of TMR modulation is somehow comparable with those of the *dI/dV* curves. This is a clear indication of the effect of QW states in the MTJs. By changing the bottom Fe-wedge layer thickness, we were able to tune the voltage dependence of the TMR ratio. From these results, we proved that the spin-transport in MTJs can be modulated by introducing QW states in the structure.

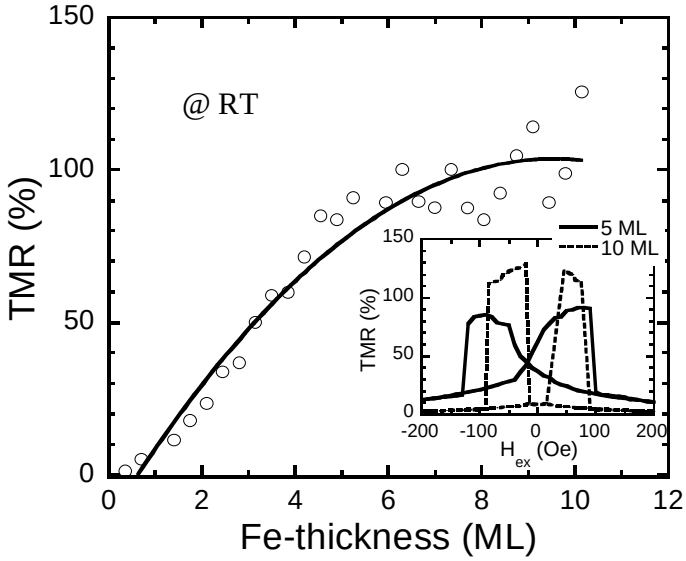


***Fig. 3.13***

*Fe-thickness dependence of TMR for MTJs with ultrathin-Fe electrodes measured at room temperature. Solid line represents background curve (quadratic function). Inset: TMR hysteresis loops of MTJs with the ultrathin-Fe thicknesses of 5 (solid line) and 10 ML (dotted line).*

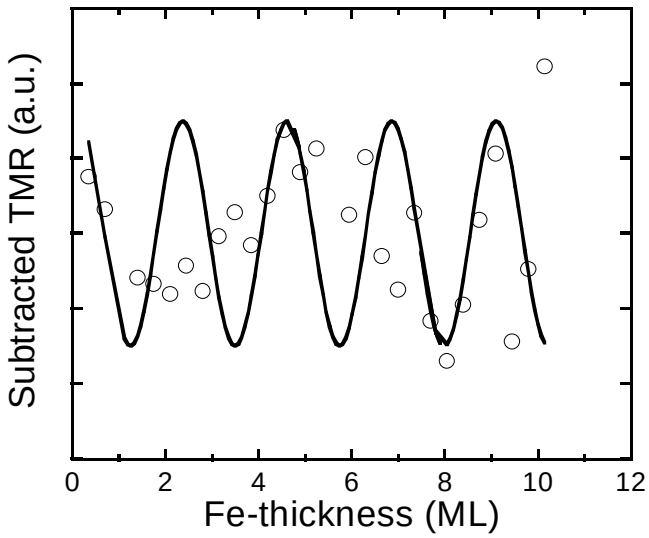


***Fig 3.14***

*Fe-thickness dependence of subtracted TMR (a difference between measured TMR and the background, as shown in Fig. 3.13) shows an oscillation with a period of 2.2 ML. Solid line is a fitting curve of a simple cosine function.*

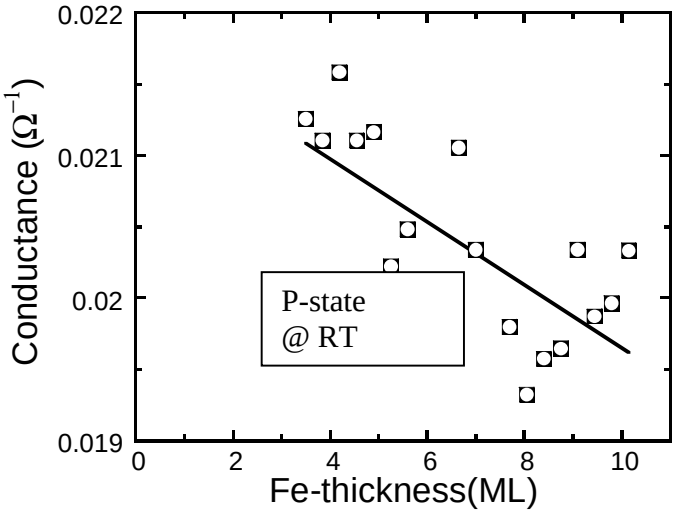


***Fig. 3.15***

*Fe-thickness dependence of parallel conductance for MTJs with ultrathin-Fe electrodes measured at room temperature. Solid line represents background obtained by a linear fitting.*

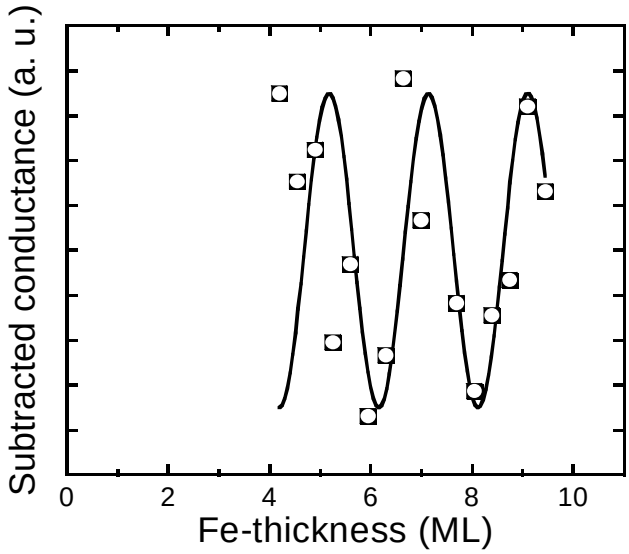


***Fig. 3.16***

*Fe-thickness dependence of the parallel conductance after a subtraction of the linear background. An oscillation with a period of 2 ML is shown. Solid curve is a fitting function.*

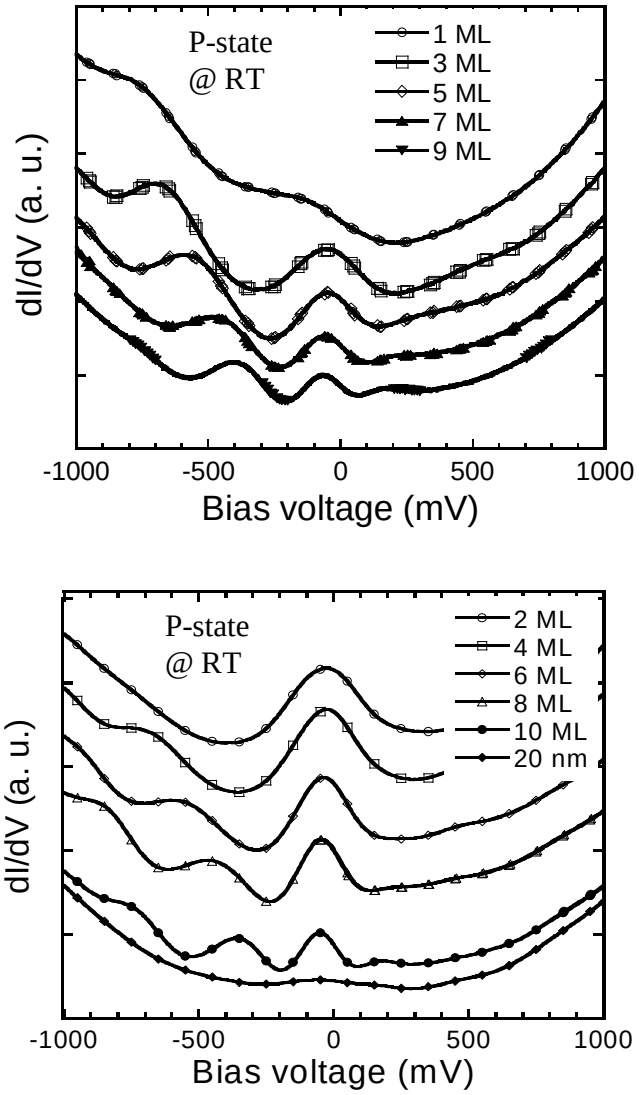


***Fig. 3.17***

*First derivative conductance spectra for MTJs having 1 to 10 ML-thickness Fe electrodes and a 20 nm Fe reference electrode measured in parallel state and at RT. MgO thickness is 20 Å. Number of the resonant peak corresponding to local maxima of dynamic conductance gradually increases with increasing ultrathin-Fe thickness.*

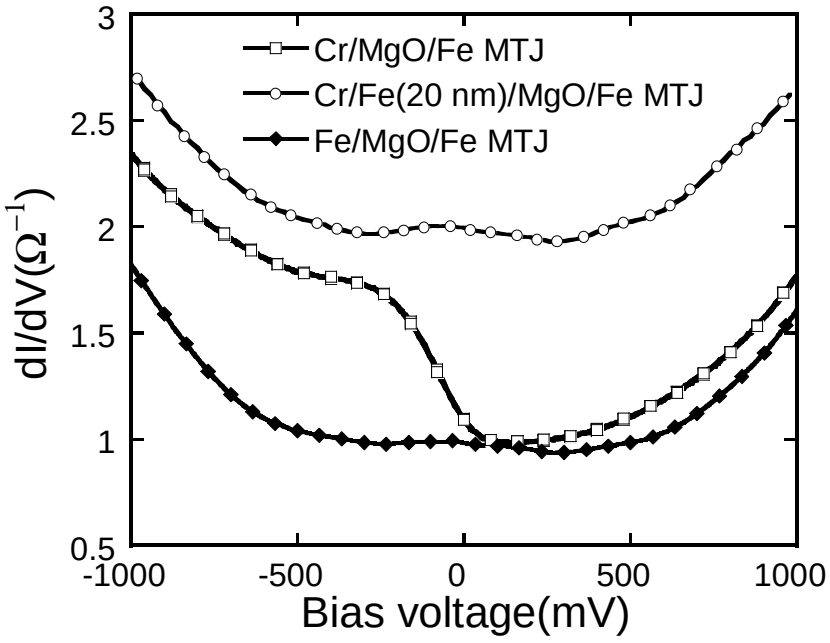


***Fig. 3.18***

*First derivative conductance curves for MTJs having different layer structures: Cr/MgO/Fe MTJ (open circles), Cr/Fe(200 Å)/MgO/Fe MTJ (open squares) and conventional Fe/MgO/Fe MTJ (solid rhomboids). The MTJs with the structure of Fe/MgO/Fe grown on Cr(001) buffer shows a similar behavior with that of the conventional Fe/MgO/Fe directly grown on MgO substrate. The MTJ with the structure of Cr/MgO/Fe shows an asymmetry in bias direction due to different interfaces.*

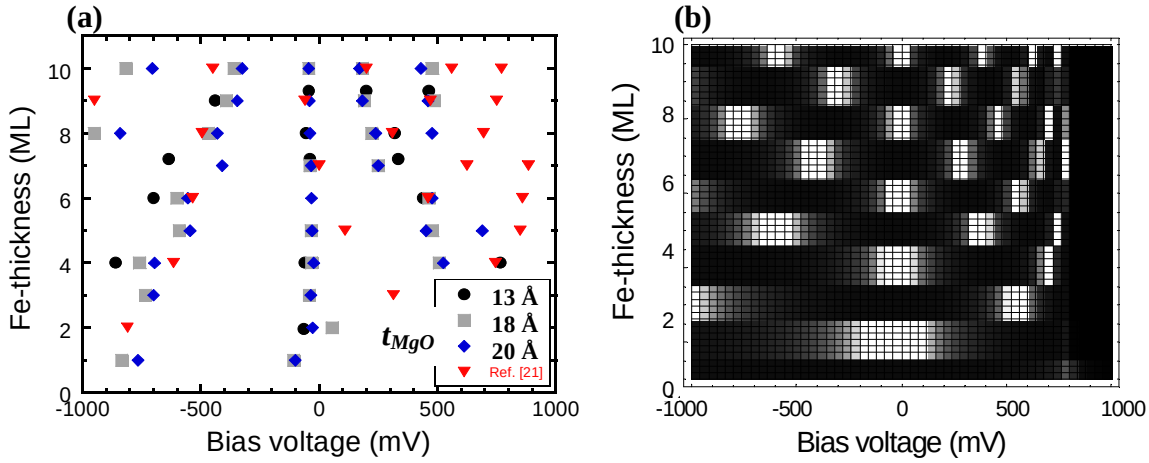


***Fig. 3.19***

*(a) The thickness dependence of the QW state energy positions for the Cr(001)/ultrathin-Fe/MgO(t)/Fe MTJs: t = 13 (black circles); 18 (gray squares) and 20 Å (blue rhomboids), and the ab-initio calculations [21] (red triangles), respectively. (b) QWs energy positions calculated using Eq. 3.5 in the text.* $\Delta\varphi_{Fe,\,MgO} + \Delta\varphi_{Fe,\,Cr} = 0.1$ *[rad].*

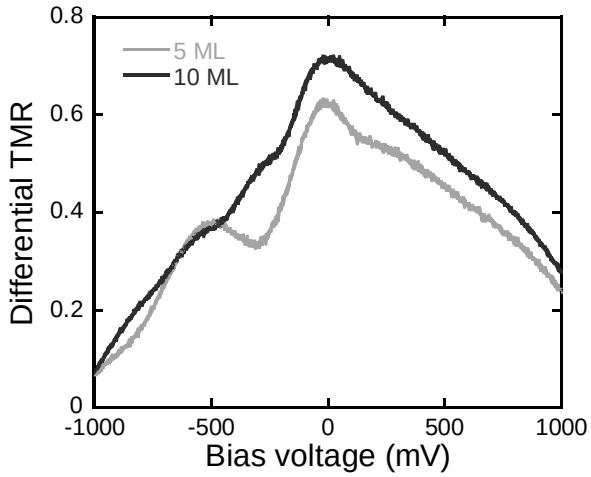


***Fig. 3.20***

*Bias dependence of differential TMR measured at RT for MTJs with ultrathin Fe thicknesses of 5 (gray line) and 10 ML (black line), and a MgO barrier thickness of 20 Å. The TMR is modulated at certain bias voltage corresponding to the quantum resonant bias position as shown in Fig. 3.18.*

## 3.4. Spin-torque diode effect in epitaxial MTJs

### 3.4.1. The details of spin-torque diode effect measurement

The spin-torque diode spectrum was investigated at room temperature. High-frequency power was modulated at 10 kHz around -15 dBm and frequency was scanned from 0.1 to 20 GHz with a revolution of 200 MHz. A *d.c.* bias voltage was also superimposed on the MTJ to change the potential energy corresponding to quantum well state energies. Spin-torque diode measurement was performed under different applied *d.c.* bias voltage ($V_{d.c.}$) of from – 400 to + 400 mV with *d.c.* bias steps of ± 40 mV, which is slightly larger than RT thermal energy and the high-frequency voltage of -15 dBm. A bias tee which is a three port network used for setting the *d.c.* bias point of some electronic components without disturbing other components was used in this measurement. The low frequency port is used to set the bias; the high frequency port passes the radio frequency signals but blocks the biasing levels; the combined port is connected to the device, which is subject to both the *d.c.* bias and *r.f.* current. In addition, a magnetic field of 800 Oe was also applied in the in-plan direction with an angle of $60^{o}$ with respect to the easy-axis of Fe(001) electrode. The measurement set up is schematically illustrated in Figure 3.21.

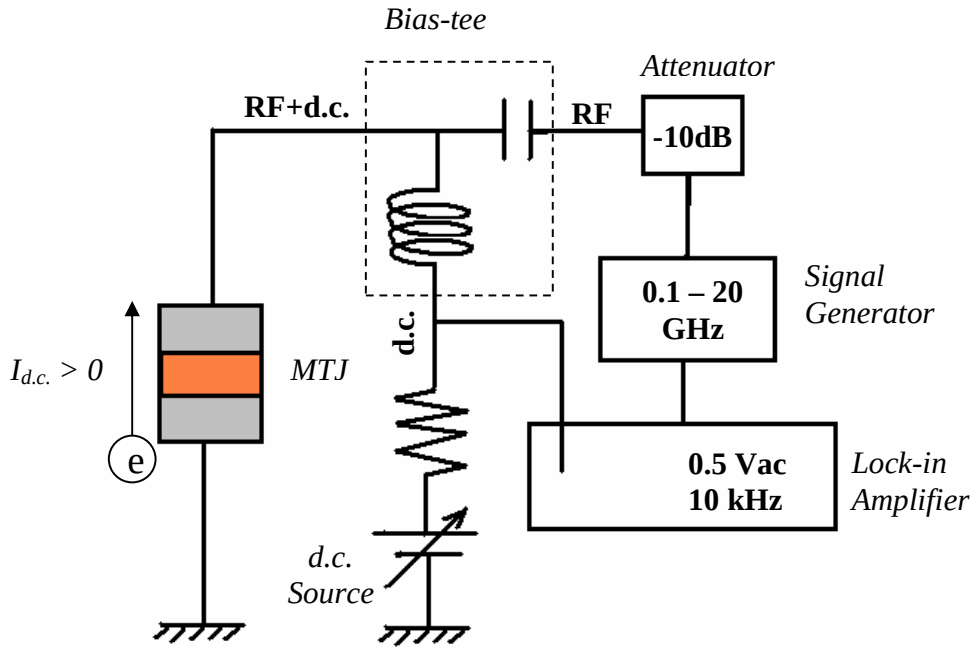


***Fig. 3.21***

*Schematic diagram of the electric circuit used for spin-torque diode measurement. A d.c. bias is superimposed with an r.f. current by using a bias-tee. A bias-tee can be viewed as an ideal capacitor from the r.f. port that allows a.c. through but blocks the d.c. bias and an ideal inductor that blocks a.c. but allows d.c. from the d.c. port. The amplitude of signal generator (0.1 – 20 GHz) is modulated at 10 kHz and then applies to the MTJ.*

### 3.4.2. Contribution of quantum well states to spin-torque diode spectrum

For the study of spin-dependent quantum resonance states effecting on the spin-transfer torque, MTJs with a small resistance and low resistance-area product (*RA*) were fabricated by reducing the thickness of the MgO barrier (1 nm). A high TMR and clear TMR hysteresis loop were obtained at room temperature as shown in the inset of Figure 3.22. However, TMR of the MTJs with ultrathin-Fe thickness of 10 ML is smaller than that of the standard epitaxial Fe/MgO/Fe having the same MgO-barrier thickness of 1 nm. One possible reason for that is formation of pinholes where local barrier thickness is zero and two Fe electrodes make direct contact. A dominantly large percentage of current flows through metallic pinholes shorts rather than tunneling through barrier, so pinholes should change the properties of the MTJ substantially.[61] Fe-thickness dependence of TMR for this sample is shown in Figure 3.22. In particular, the TMR is rapidly decreased when the ultrathin-Fe thickness becomes less than 7 ML. The same analyzing processes, i.e. subtracting to background curve from TMR data points and fitting the subtracted TMR data with a single cosine function, was performed and shown in Figure 3.23. The fitting curve (solid line in Fig. 3.23) also shows a period of 2 ML as the results of MTJs with thicker MgO-barrier. From these results it could be ensure that the quantum interference effect is an intrinsic property of the ultrathin-Fe layer.

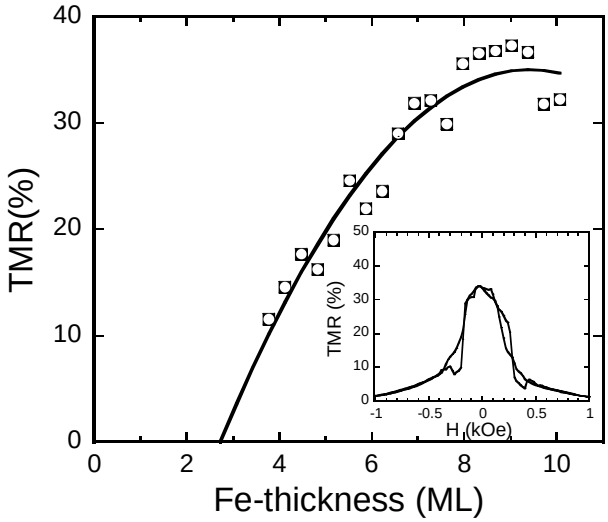


***Fig. 3.22***

*MgO thickness dependence of TMR for epitaxial MTJs with a MgO-barrier thickness of 10 Å measured at room temperature. Solid line represents background curve, which was fitted by a quadratic function. The inset shows a represent hysteresis loop of TMR for MTJs with an 10 ML-thick Fe electrode.*

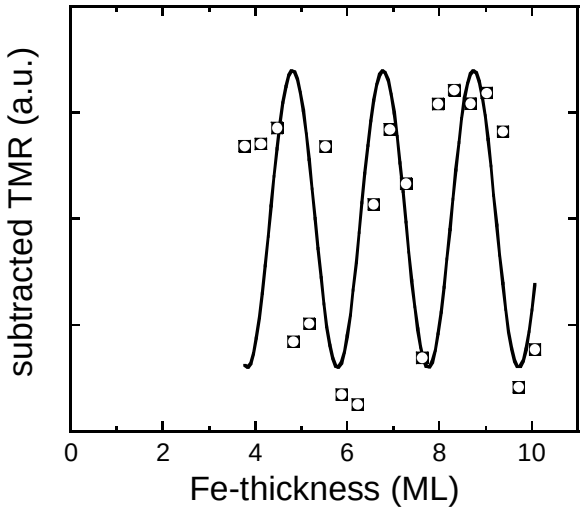


***Fig. 3.23***

*Oscillatory component of TMR (after a subtraction of a quadratic background) as a function of Fe thickness for epitaxial MTJs with a MgO-barrier of 10 Å measured at room temperature. Solid line is the fitting curve with a single period of 2 ML.*

The quantum well states were also observed in the MTJ with the very thin MgO-barrier of 10 Å. To evaluate effect of the QWs on spin-torque properties of the MTJ, spin-torque diode measurement was performed under different applied *d.c.* bias voltages. First, the spin-torque diode spectra were measured with different angles of in-plan magnetic field under zero *d.c.* bias. The magnetic field of 1200 Oe was set in-plan of the MTJ, at which two magnetizations of Fe electrodes are not completely parallel. In the samples of this study, the Fe/Cr/Fe synthesis antiferromagnetic multilayer acts as a pinned layer, while the bottom ultrathin-Fe layer acts as a free layer, whose magnetization can be changed. By changing angle of the in-plan magnetic field relatively to the easy-axis of Fe(001) electrodes, one can change the angle between the pinned layer and free layer as well as frequency of the precession. The spin-torque diode spectra of the MTJ with a 10 ML thick Fe electrode measured under different angles are shown in Figure 3.24. The spectra are shifted vertically for clarify. In all the spectra, one or several resonant peaks are observed on background signals caused by nonlinear *I-V* characteristics of the tunneling conductance. On increasing the in-plan magnetic field angle relatively to the Fe[001] direction, both the peak shape and resonant frequency are changed. For the angle of $0^o$, the main resonance peak occurred at high frequency of about 11GHz with a dispersion shape which favors to effective field like-torque. However, when the field made an angle of $60^o$ the spectrum showed a clear resonant peak at 8 GHz and the peak shape was changed into a Lorentzian shape which was contributed to spin-transfer torque.[23] According to authors of Ref. [23], there are two kinds of torque at zero bias: a spin-transfer torque that rotates magnetization of the free layer in-plane direction and plays a dominant role in magnetization reversal; and a field-like torque that rotates magnetization of the free layer perpendicularly to the film plane.

The contribution of spin-transfer torque to the spin-torque diode spectrum in different magnetic field was also investigated. In this measurement, the angle of the in-plan magnetic field was fixed at $60^o$ relatively to the Fe[001] direction. The spectra measured under zero bias and various magnetic fields were shown in Figure 2.25. A clear blue-shift was observed when the in-plan field increases from 700 Oe to 1500 Oe. Some additional peaks were also appeared in the spectra measured under magnetic fields less than 1000 Oe. It should be noted that many other samples similar to that used in this measurement showed more complicated spectra, which is found to be mainly due to magnetization distribution inside the magnetic cell or different precession modes of magnetizations of the free and pinned layers. The frequency of the

resonance position as a function of magnetic field is plotted in Figure 3.26. The dashed line is the fit to the data using Kittel's equation:[63]

$$f = \gamma' \left[ \left( H_c + \left| H_{dip} + H_{ex} \right| \right) \left( H_c + H_d + \left| H_{dip} + H_{ex} \right| \right) \right]^{\frac{1}{2}} \qquad \text{(Eq. 3.6)}$$

where γ is the gyromagnetic ratio (γ'= - γ/2π), $H_c$ is the coercivity, $H_d$ is the demagnetization field perpendicular to the free-layer plane, Hdip is the dipolar field from the pinned layer and $H_{ex}$ is the applied external magnetic field. The coercivity ($H_c$) of 0.3 kOe was obtained from TMR hysteresis loop. Therefore, the fitting to Kittel's equation gives γ' = 2.86, $H_{dip}$ = 0.7 kOe and $H_d$ = 9.4 kOe.

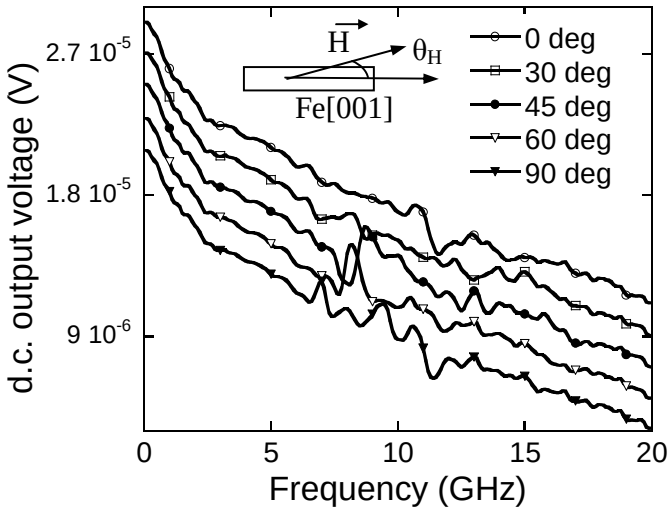


***Fig. 3.24***

*Spin-torque diode spectra of the MTJ with a 10 ML thick Fe electrode and 10 Å thick MgO-barrier measured under an in-plan magnetic field with various angles. The optimum curve is obtained under the angle of 60$^o$ from the Fe[001] direction.*

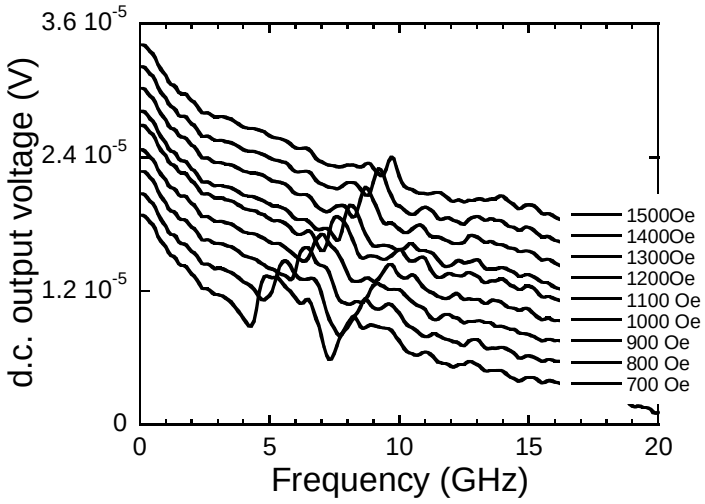


***Fig. 3.25***

*Spin-torque diode spectra of the MTJ with 10 ML thick Fe electrode and 10 Å-thick MgO barrier measured various in-plane magnetic fields formed an angle of 60$^o$ to Fe[001] direction. The resonant frequency strongly depends on applied magnetic field.*

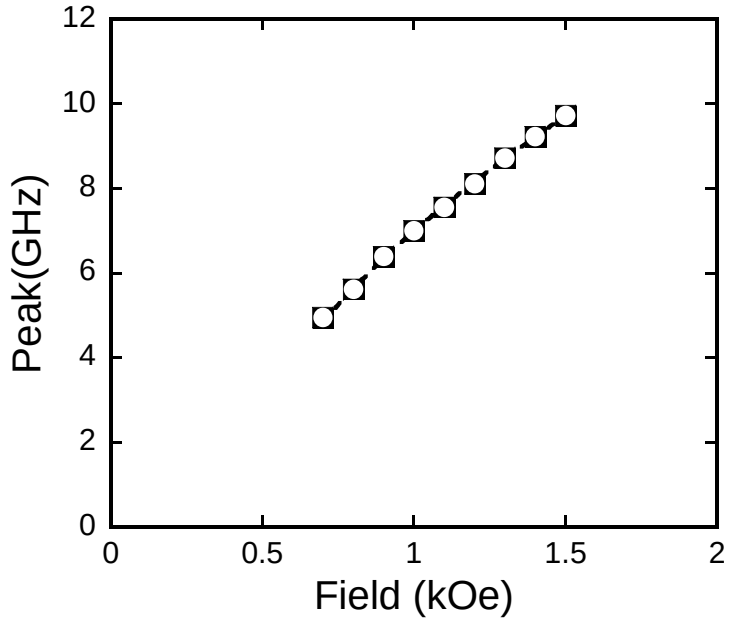


***Fig. 3.26***

*The magnetic field dependence of resonant frequency corresponding to the main peak in the spin-torque diode spectra for the MTJ with 10 ML-thick Fe electrode and 10 Å-thick MgO barrier. The dashed line is the fit to the data using Kittel's equation (Eq. 3.6).*

The spin-transfer diode spectra under different applied *d.c.* bias voltage ($V_{d.c.}$) of from – 400 to + 400 mV were measured to evaluate the effect of the QW sates on spin torque properties. In the measurement, a magnetic field of 800 Oe was applied in-plane direction with an angle of $60^{o}$ with respect to the easy-axis of Fe(001) electrode. The changed *d.c.* bias voltage was swept by steps increment/decrement of ± 40 mV, which is slightly larger than *RT* thermal energy (25 meV) and the high-frequency voltage amplitude for -15 dBm.

The spin-torque diode spectra obtained under various *d.c.* bias voltages are shown in Figure 3.27. For all applied $V_{d.c.}$, clear Lorentzian spectra were observed at 5.2 GHz for low bias region (-200 to +200 mV), where a ferromagnetic resonance of the free layer magnetization was excited by the spin torque. For the MTJ with a very thin MgO-barrier thickness of 10 Å, it should be noted that dynamic conductance also oscillates in this applied bias regime as shown in Figure 3.28. Over all spectra, the resonant frequency did not depend on the applied *d.c.* bias in measured bias region. Applied $V_{d.c.}$ dependence of the peak height is shown in Figure 3.29. Comparing with the result of *dI/dV* curve, which showed a clear oscillation as it is shown in Figure 3.28, a small bias voltage (less than 150 mV) causes significant reduction of the peak height. Moreover, it was enhanced at around -400 and 300 mV. This behavior is different in comparing with that of the sample without of QWs in Ref. [45]. Kubota *et al.* showed that $V_{d.c.}$ has non-monotonic bias dependence. Near zero bias, it shows a linear dependence on bias. However, at larger biases it rapidly increases with negative bias and slowly decreases with positive bias. This strong nonlinear behavior was attributed to a nonlinear bias dependence of the MTJ conductance. The different torque properties between MTJs with and without QWs can be an intrinsic property of QWs affecting on spin-polarization as well as spin-torque.

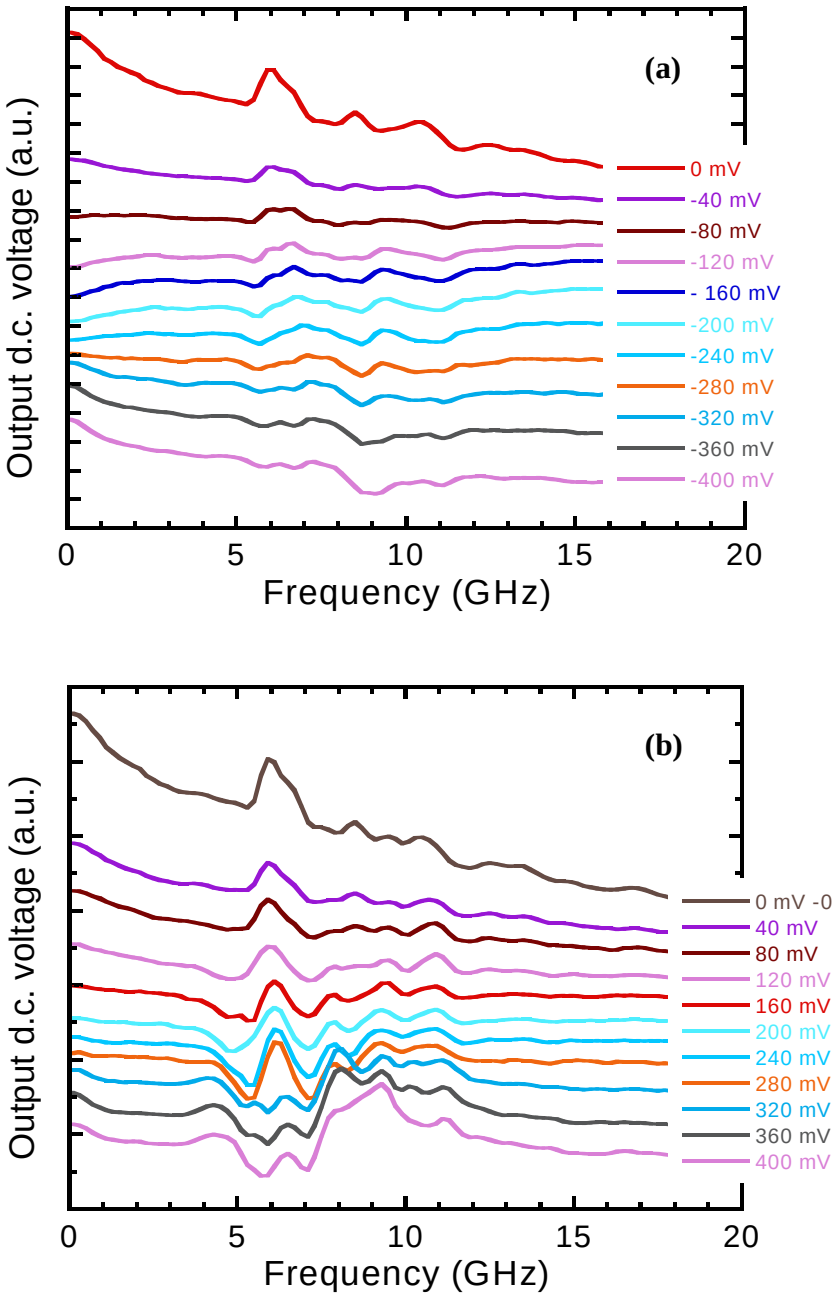


***Fig. 3.27***

*Spin-torque diode spectra measured under an external magnetic field of 800 Oe and a different angle of 60$^{o}$ from easy-axis of Fe(001) and various d.c. bias voltages: (a) negative bias, (b) positive bias.*

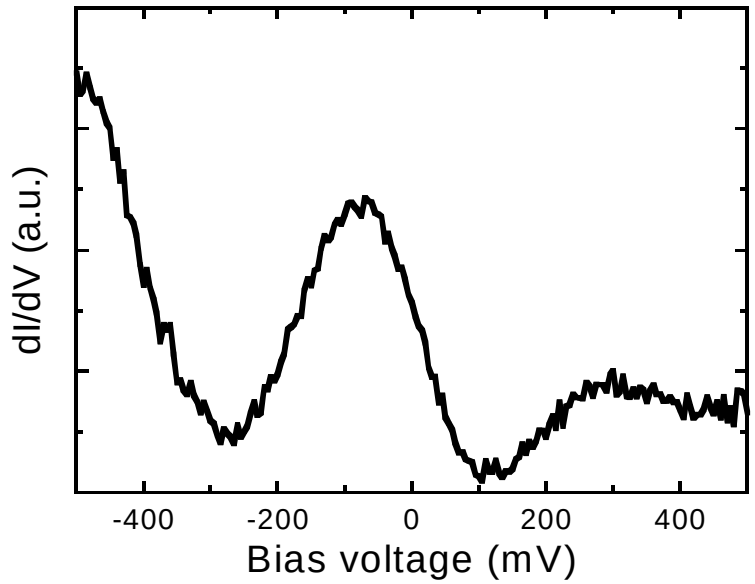


***Fig. 3.28***

*Parallel dynamic conductance oscillates as a function of bias voltage for the MTJ with a MgO barrier thickness of 10 Å and $t_{Fe}$ = 10 ML.*

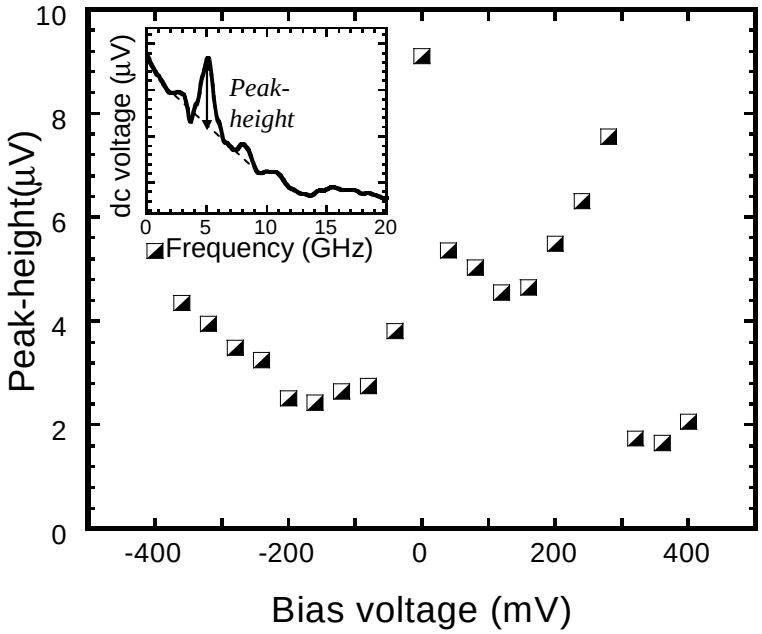


***Fig. 3.29***

*Output d.c voltage peak height, as marked by the arrow in the inset, depends on applied d.c. bias voltages. Output d.c. voltage is enhanced at the bias voltages corresponding to QWs energies of -400 and 300 mV.*

# CHAPTER 4. CONCLUSIONS

To realize new possibilities for future data storage applications with ultimate speeds and density, tunneling magnetoresistance ratio (TMR) of magnetic tunnel junctions (MTJs) have been rapidly improved by optimizing functions of materials and/or sample growth techniques. However, the highest experimental TMR is still much smaller than that of theoretical predictions. The TMR effect is also known to be sensitive to layer interfaces due to quantum effects such as a scattering or interference of tunneling electrons. By investigating origins of spin-dependent scatterings which may cause a reduction of TMR in the MgO-based MTJs, and by introducing QWs formed in an ultrathin metallic layers to improve TMR ratio, the author obtained the following results which fulfill the purposes of the dissertation.

## 4.1. Kondo and magnon effect in MgO-based MTJs

To investigate the influence of metallic-insulator interfaces on the transport properties in the MgO-based MTJs, a series of the single crystal MTJs with structure of Fe(001)/MgO(001)/Fe(001) and textured MTJs with structure of Co60Fe20B20/MgO/Co70Fe30Bx by adding boron with various concentrations (x) into top magnetic electrodes were fabricated by epitaxy and magnetron sputtering methods, respectively. Electron tunneling spectroscopy was systematically measured for the MTJ structure of Co60Fe20B20/textured MgO(001)/Co70Fe30Bx MTJs under various temperatures from 2 to 300 K. The dynamic conductance spectra show the zero-bias anomaly dip which was attributed to Kondo effect due to a spin interaction of the localized spin of a Kondo impurity with the spin of surrounding conduction electrons. This Kondo effect was significant at low temperatures and caused a reduction in the achievable TMR ratio compared with the highest predicted value in the MgO-based MTJs. Employing the model, called Fano interference, that treats the interference between a direct tunneling and a tunneling via a magnetic impurity in the barrier, the dip structure in the dynamic conductance was well reproduced. From the fittings, the Kondo temperature was estimated to be about 80 - 100 K for our samples. The absence of the boron concentration dependence of the ZBA intensity and the absence of the ZBA in the single crystalline MTJs suggested that magnetic impurities (Fe, Co or Mn) diffused into the MgO barrier through defects could be an origin of the effect.

The inelastic tunneling of electrons in magnetic tunnel junctions (MTJs) due to low energy excitations such phonons and magnons may lead to an enhancement low bias conductance by

opening new conductance channels above and below the Fermi energy. To study the magnon effect and its contributions to the properties of the MgO-based MTJs, the author also measured detailed temperature dependences of conductance and second derivative conductance on the same samples which were used in measurements of the Kondo effect.

The results showed broad peak structure from 5 mV to 200 mV contained additional peaks at 23, 54 and 85 mV which were assigned to excitation of magnons except that at 85 mV. The magnetic origin of those peaks agreed with expected difference in the peak intensity according to a magnetization configurations and boron concentrations (TMR ratio). In antiparallel configuration, the intensity of the $d^2I/dV^2$ spectra is systematically reduced from MTJ without boron to 2 % of boron inclusion. The peak positions and shapes were remained almost the same. But low energy broad peak intensity as considerable reduced for AP configuration. Therefore, we can conclude that inclusion of the boron did not show significant modification in magnon dispersion but it affected to the spin polarization of the tunneling electrons. Then, a change in the TMR ratio resulted relative significance of the magnon assisted spin-flip process to the conduction. The addition of B may result in a reduced $T_c$ of the ferromagnetic electrodes and consequently should reduce the energy of excited magnons. However, such changes were not observed in our experiment. This result proposes a negligible change in the exchange constant by an inclusion of such small amount of boron atoms.

The temperature dependence of the sample TMR ratio can be explained by both *2D* and *3D* magnon excitations. However, abrupt increase in the second derivative conductance at very low biasing voltage in the antiparallel configuration suggests important role of the surface *2D* magnon excitation.

### 4.2. Quantum resonant effect in epitaxial MgO-based MTJs

Author has succeeded in making the MTJ with TMR as high as 200% at room temperature. An oscillatory barrier thickness dependence of TMR was also observed. The thickness dependence of TMR was well fitted by a simple cosine function with an oscillation period of 3.5 Å after subtraction of smooth background. It is an evidence of existing quantum interference effect in the MTJ.

For the study of the effect of spin-dependent quantum resonant states on the spin-transfer torque properties, MTJs with small resistance and low resistance-area product (*RA*) were fabricated by reducing the thickness of the MgO barrier (10 Å) and introducing an ultrathin-Fe electrode. A high TMR and clear TMR hysteresis loop were obtained at room temperature. The TMR also oscillates as a function of the ultrathin-Fe. The TMR as a function of the Fe layer thickness was well fitted by a single cosine function for the MTJs with different MgO barriers of 10 and 20 Å after background correction. The fitting curves showed a same oscillatory period of 2 ML. From these results it could be ensured that the quantum interference effect is an intrinsic property of the ultrathin-Fe layer.

The author also investigated the differential conductance as a function of bias voltage (*dI/dV* spectrum) of the MTJs with different ultrathin Fe electrode grown on crystalline Cr(001) buffer layer. The TMR ratio is clearly modulated at bias voltages corresponding to the local maxima in first derivative conductance spectra. The oscillations of dynamic conductance and TMR are also remarkable evidences of the QW states formed in the ultrathin Fe layers in MTJs. In these MTJs, electronic structures of the ultrathin Fe layer are definitely modified by the QW states.

### 4.3. Contribution of quantum well states to spin-torque diode spectrum in epitaxial MgO based MTJs

The spin-torque diode spectra were observed under different angles of in-plane magnetic fields for the MTJ with a very thin MgO barrier of 10 Å and ultrathin-Fe electrode. The clear spectra with a single peak of the output *d.c.* voltage at the FMR frequency of the free-layer magnetization. The spin-torque diode spectra were also investigated under various *d.c.* bias voltages. The peak height of output *d.c.* voltage in these spectra was seems to be enhanced at the bias corresponding to the QWs energy positions such as around -400 and 300 mV. From these observations of the bias dependence of conductance, QWs energy position and peak-height of spin-torque diode spectrum, it can be suggested that the spin-torque was significantly influenced by the QWs formed in the ultrathin-Fe electrode of the MTJ.

## ACKNOWLEDGEMENTS

This doctoral study has been possible due to many persons who directly and indirectly helped me progress in the advanced direction. In the first place, I am deeply grateful to my Ph.D supervisors, Professor Yoshishige Suzuki (professor, Osaka University, Japan) and Professor Nguyen Xuan Phuc (professor, Institute of Materials Science - IMS, Hanoi, Vietnam) for granting me an exciting Ph.D topic and for mentoring the subsequent research efforts. I respectfully appreciate their role in instructing my research and analytical skills, giving me freedom to try new methods and patiently supporting me during numerous struggles. I had a deeply satisfying learning period in Osaka University lab.

I would like to take the opportunity to thank Mr. Takayuki Nozaki (assistant professor, Osaka University) and Dr. Nguyen Huy Dan (associate professor of IMS, Viet Nam) for giving me their continual advice, useful discussion, wisdom, and encouragement throughout my research in Osaka and IMS. Appreciations are also due to them for equipping me with much needed knowledge of experimental systems.

I take pleasure in acknowledging Dr. Shinji Yuasa, Dr. Hitoshi Kubota, Dr. Akio Fukushima and other members of Spintronics Research Group in AIST for giving me access to their group and training me on thin-film epitaxy growth and micro-fabrication. I also wish to thank them for giving their opinions and suggestions about some of the complex results we observed during this doctoral study.

I am grateful to Mr. Hiroki Maehara and Mr. David D. Djayaprawira in Canon ANELVA Corporation for providing high-quality CoFeB/MgO/CoFe MTJs for the studies on Kondo and magnon effects.

I gratefully acknowledge time spared by Prof. M. Shiraishi, Prof. H. Kasai, Prof. H. Nakanishi and Ms. E. Minamitani in Osaka University, Prof. H. Itoh in Kansai University, and Prof. K. Rhie and T.-S. Kim in Korea for giving their cooperation and instructions.

I am thankful to all former and present lab mates in Osaka and IMS for their role in improving my experimental skills. These skills provided a strong foundation I always benefited from. I am also indebted to a number of friends who have assisted me in several crucial stages.

I express my thanks to Ms. Rie Hasegawa, Ms. Yumi Oda (secretaries, Osaka University), Ms. Kazuko Sato (secretary, AIST) and staffs of Graduate School of Engineering Science, Osaka University for their kindly help and support.

I am thankful to the Program of cooperative education between Institute of Materials Science, VAST and Osaka University, Vietnamese Ministry of Education and Training and it Project of "Training Scientific and Technical Cadres in Institutions Overseas with the State Budget", and Osaka University Global COE (GCOE) Program for funding this dissertation work.

I express my gratefulness towards my parents for giving me the opportunity to explore the world around me. Finally, I wish to thank my special friend and wife, Ms. Nguyen Thi Hue, for her continuous support, understanding and taking extra burden. I am thankful to my little sons, Do Nguyen Vu and Do Nguyen Bao to bear my long absence from home.

## REFERENCES


[1] M. Jullière, Phys. Lett. A **54**, 225 (1975).

[2] T. Miyazaki and N. Tezuka, J. Magn. Magn. Mater. **139**, L231 (1995).

[3] J. S. Moodera, L. R. Kinder, T. M. Wong, and R. Meservey, Phys. Rev. Lett. **74**, 3273 (1995).

[4] D. Wang, C, Nordman, J. Daughton, Z. Qian, and J. Fink, IEEE Trans. Magn. **40**, 2269 (2004).

[5] W. H. Butler, X.-G. Zhang, T. C. Schulthess and J. M. McLaren, Phys. Rev. B **63**, 054416 (2001).

[6] J. Mathon and A. Umerski, Phys. Rev. B **63**, 220403 (2001).

[7] S. Yuasa, T. Nagahama, A. Fukushima, Y. Suzuki, and K. Ando, Nature Mater. **3**, 868 (2004).

[8] S. S. P. Parkin, C. Kaiser, A. Panchula, P. M. Rice, B. Hughes, M. Samant, and S.-H. Yang, Nature Mater. **3**, 862 (2004).

[9] T. Nagahama, S. Yuasa, E. Tamura, and Y. Suzuki, Phys. Rev. Lett. **95**, 086602 (2005).

[10] Y. M. Lee, J. Hayakawa, S. Ikeda, F. Matsukura, and H. Ohno, Appl. Phys. Lett. **90**, 212507 (2007).

[11] D. D. Djayaparawira, K. Tsunekawa, M. Nagai. H. Maehara, S. Yamagata, N. Watanabe, S. Yuasa and K. Ando, Appl. Phys. Lett. **86**, 092502 (2005).

[12] X.-G. Zhang and W. H. Butler, Phys. Rev. B. **70**, 172407 (2004).

[13] S. Ikeda, J. Hayakawa, Y. Ashizawa, Y. M. Lee, K. Miura, H. Hasegawa, M. Tsunoda, F. Matsukura and H. Ohno, Appl. Phys. Lett. **92**, 082508 (2008).

[14] C. Heiliger, P. Zahn, B. Yu Yavorsky, and I. Mertig, Phys. Rev. **B**. 73, 214441 (2006).

[15] J. Kondo Progr. Theore. Phys. (Kyoto) **2**, 772 (1962).

[16] D. L. Cox and A. Zawadowski, Advances in Physics **47**, 599 (1998).

[17] J. E. Ortega, F. J. Himpsel, G. J. Mankey, R. F. Willis, Phys. Rev. B **47**, 1540 (1993).

[18] S. Yuasa, T. Nagahama, and Y. Suzuki, Science 297, **234** (2002).

[19] P. LeClair, B. Hoex, H. Wieldraaijer, J. T. Kohlhepp, H. J. M. Swagten, and W. J. M. de Jonge, Phys. Rev. B **64**, 100406 (2001).

[20] Jagadeesh S. Moodera, Janusz Nowak, Lisa R. Kinder, Paul M. Tedrow, J. M. Rene, van de Veerdonk, A. Smits Bart, Maarten van Kampen, Henk J. M. Swagten, and Wim J. M. de Jonge, Phys. Rev. Lett. **83**, 3029 (1999).

[21] Z. Y. Lu, X. –G. Zhang, and S. T. Pantelides, Phys. Rev. Lett. **94**, 207210 (2005).

[22] H. Kubota, A. Fukushima, Y. Ootani, S. Yuasa, K. Ando, H. Maehara, K. Tsunekawa, D. D. Djayaprawira, N. Tanabe, and Y. Suzuki, Appl. Phys. Lett. **89**, 032505 (2006).

[23] A. A. Tulapurkar, Y. Suzuki, A. Fukushima, H. Kubota, H. Maehara, K. Tsunekawa, D. D. Djayaprawira, N. Watanabe, S. Yuasa, Nature **438**, 339 (2005).

[24] A. M. Deac, A. Fukushima, H. Kubota, H. Maehara, Y. Suzuki, S. Yuasa, Y. Nagamine, K. Tsunekawa, D. D. Djayaprawira, and N. Watanabe. Nature Physics **4**, 803 (2008).

[25] J. A. Appellbaum, Phys. Rev. **154**, 633 (1967).

[26] F. Mezei, Phys. Letters **25A**, 534 (1967).

[27] F. Mezei and A. Zawadowski, Phys. Rev. B. **3**, 3127 (1971).

[28] K. Hattori, Y. Hariyama and K. Miyake, J. Phys. Soc. Japan **74**, 3306 (2005); and J. Phys. Soc. Japan **74**, 49 (2005).

[29] E. Minamitani, H. Nakanishi, W. A. Diño, and H. Kasai, J. Phys. Soc. Japan **78**, 084705 (2009).

[30] P. Nozieres, J. Low Temp. Phys. **17**, 31 (1974).

[31] K. I. Lee, S. J. Joo, J. H. Lee, K. Rhie, T.-S. Kim, W. Y. Lee, K. H. Shin, B. C. Lee, P. LeClair. J.-S. Lee and J.-H. Park, Phys. Rev. Lett. **98**, 107202 (2007).

[32] J. S. Moodera, J. Nowak, and R. J. M. van de Veerdonk, Phys. Rev. Lett. **80**, 2941 (1998).

[33] J. Murai, Y. Ando, M. Kamijo, H. Kubota, and T. Miyazaki, Jpn. J. Appl. Phys. **38**, L1106 (1999).

[34] T. Miyazaki, T. Yaoi, and S. Ishio, J. Magn. Magn. Mater. **98**, L7 (1991).

[35] A. M. Bratkovsky, Phys. Rev. B **56**, 2344 (1997).

[36] T. Balashov, A. F. Takacs, M. Dane, A. Ernst, P. Bruno, and W. Wulfhekel, Phys. Rev. B, **78**, 174404 (2008).

[37] R. Matsumoto, Y. Hamada, M. Mizuguchi, M. Shiraishi, H. Maehara, K. Tsunekawa, D. D. Djayaprawira, N. Watanabe, T. Nagahama, A. Fukushima, H. Kubota, S. Yuasa, and Y. Suzuki, Solid State Commun. **136**, 611 (2005).

[38] K. Ono, T. Daibou, S. J. Ahn, Y. Sakuraba, T. Miyakoshi, T. Morita, Y. Kikuchi, M. Oogane, Y. Ando, and T. Miyazaki, J. Appl. Phys. **99**, 08A905 (2006).

[39] V. Drewello, J. Schamalhorst, A. Thomas, and G. Reiss, Phys. Rev. B **77**, 014440 (2008).

[40] T. Nozaki, N. Tezuka, and K. Inomata, Phys. Rev. Lett. **96**, 027208 (2006).

[41] T. Niizeki, N. Tezuka, and K. Inomata, Phys. Rev. Lett. **100**, 047207 (2008).

[42] J. C. Slonczewski, Phys. Rev. B **39**, 6995 (1989).

[43] L. Berger, Phys. Rev. B **54**, 9535 (1996).

[44] F. Greullet, C. Tuisan, F. Montaigne, M. Hehn, D. Halley, O. Bengone, M. Bowen, and W. Weber, Phys. Rev. Lett. **99**, 187202 (2007).

[45] H. Kubota, A. Fukushima, K. Yakushiji, T. Nagahama, S. Yuasa, K. Ando, H. Maehara, Y. Nagamine, K. Tsunekawa, D. D. Djayaprawira, N. Watanabe and Y. Suzuki, Nature **4**, 37 (2008).

[46] T. Kawasaka and A. Okiji, J. Appl. Phys. **86**, 6970 (1999).

[47] W. A. Diño, H. Kasai , Thin Solid Films **509**, 168 (2006).

[48] T. S. Kim and Hershfield, Phys. Rev. B **63**, 245326 (2001).

[49] S. Zhang, P. M. Levy, A. C. Marley, and S. S. P. Parkin, Phys. Rev. Lett. **79**, 3744 (1997).

[50] J. G. Adler, Solid State Comm. **7**, 1635 (1969).

[51] S. Nishioka, R. Matsumoto, H. Tomita, T. Nozaki, Y. Suzuki, H. Itoh, and S. Yuasa, Appl. Phys. Lett. **93**, 122511 (2008).

[52] D. C. Tsui, R. E. Dietz, and L. R. Walker, Phys. Rev. Lett. **27**, 1729 (1971).

[53] X. G-.Zhang, Y. Wang, and X. F. Han, Phys. Rev. B **77**, 144431 (2008).

[54] R. Matsumoto, A. Fukushima, T. Nagahama, Y, Suzuki, K. Ando, and S. Yuasa, Appl. Phys. Lett. **90**, 252506 (2007).

[55] E. L. Wolf, Principles of electron tunneling spectroscopy (Oxford University, New York 1989).

[56] Do Bang, T. Nozaki, D. D. Djayaprawira, M. Shiraishi, Y. Suzuki, A. Fukushima, H. Kubota, T. Nagahama, S. Yuasa, H. Maehara, K. Tsunekawa, Y. Nagamine, N. Watanabe, and H. Itoh, J. Appl. Phys. **105**, 07C924 (2009).

[57] Y. Suzuki, T. Katayama, P. Bruno, S. Yuasa and E. Tamura, Phys. Rev. Lett. **80**, 5200 (1998).

[58] D. A. Papaconstantopoulos, Handbook of the Band Structure of Elemental Solids (Plenum, New York 1986).

[59] T. Nagahama, S. Yuasa, Y. Suzuki and E. Tamura, J. Appl. Phys. **91**, 7035 (2002).

[60] C. Heiliger, Peter Zhan, Bogdan Yu. Yavorsky and Ingrid Mertig, Phys. Rev. B. **73**, 214441 (2006).

[61] I. Theodonis, A. Kalitsov, and N. Kioussis, Phys. Rev. B **76**, 224406 (2007).

[62] S. –Z. Shang, and D. A. Rabson, J. Appl. Phys. **95**, 557 (2004).

[63] C. Kittel, Introduction to Solid State Physics, Ch. 16 (John Wiley & Sons, Singapore, 1996).

# INDEX

**Definitions of symbols and terms in this thesis are also summarized**

## PUBLICATIONS

[*Published*]

1. Do Bang, T. Nozaki, D. D. Djayaprawira, M. Shiraishi, Y. Suzuki, A. Fukushima, H. Kubota, T. Nagahama, S. Yuasa, H. Maehara, K. Tsunekawa, Y. Nagamine, N. Watanabe, and H. Itoh, "*Inelastic tunneling spectra of MgO barrier magnetic tunneling junctions showing large magnon contribution*," J. Appl. Phys. 105, 07C924 (2009).
2. Do Bang, T. Nozaki, Y. Suzuki, K. Rhie, T.-S. Kim, A. Fukushima, S. Yuasa, E. Minamitani, H. Nakanishi, and H. Kasai, "*Study of Kondo effect in MgO-based magnetic tunnel junctions by electron tunneling spectroscopy*," Journal of Physisc: Conference Series 200, 052004 (2010).

[*In preparation*]

3. Do Bang, T. Nozaki, and Y. Suzuki "*Strong quantum interference effect in fully epitaxial Cr/Fe/MgO/Fe magnetic tunnel junctions with Fe ultrathin electrodes at room temperature*".

## LIST OF CONFERENCE PRESENTATIONS

[*oral presentation*]

1. Do Bang, S. Nishioka, T. Nozaki, S. Suzuki, K. Rhie, H. Kubota, A. Fukushima and S. Yuasa "*Magnetic scattering in CoFeB/MgO/CoFe magnetic tunnel junctions*," The Asia Magnetism Conference (AMC) 2008, BA-2, Busan, Korea (Dec. 2008)

2. Do Bang, T. Nozaki, Y. Suzuki, K. Rhie, T.-S. Kim, A. Fukushima, S. Yuasa, E. Minamitani, H. Nakanishi, and H. Kasai "*Study of Kondo effect in MgO-based magnetic tunnel junctions by electron tunneling spectroscopy*," The International Conference of Magnetism (ICM) 2009, Fr-JB4-03, Karlsruhe, Germany (July, 2009).

3. Do Bang, T. Nozaki, and Y. Suzuki "*Strong quantum interference effect in fully epitaxial Cr/Fe/MgO/Fe magnetic tunnel junctions with Fe ultrathin electrodes at room temperature*". The 55$^{rd}$ Annual Conference on Magnetism and Magnetic Materials (MMM) 2010, HB-03, Atlanta, Georgia (Nov. 2010), accepted

[*poster presentation*]

4. Do Bang, T. Nozaki, Y. Suzuki, M. Shiraishi, H. Kubota, A. Fukushima, and S. Yuasa "*Kondo effect in CoFeB/MgO/CoFe magnetic tunnel junctions*," The 2nd IEEE Nanotechnology Materials and Devices Conference (NMDC) 2008, Tu-P36, Kyoto, Japan (Oct. 2008).

5. Do Bang, T. Nozaki, D. D. Djayaprawira, M. Shiraishi, Y. Suzuki, A. Fukushima, H. Kubota, T. Nagahama, S. Yuasa, H. Maehara, K. Tsunekawa, Y. Nagamine, N. Watanabe, and H. Itoh, "*Inelastic tunneling spectra of MgO barrier magnetic tunneling junctions showing large magnon contribution*," The 53rd Annual Conference on Magnetism and Magnetic Materials (MMM) 2008, BR-05, Austin, Texas (Nov. 2008)

6. Do Bang, T. Nozaki and Y. Suzuki "*Study of resonant effect in fully Epitaxial Au/ultrathin-Fe/MgO/Fe magnetic tunnel junctions*," The International conference on Core Research and Engineering Science of Advanced Materials, PSII-29, Osaka, Japan (June, 2010).